ALEPH 93-30
PHYSIC 93-21
A. Falvard et al.
17.02.1993

Production and Semileptonic Decays of Heavy Quarks at the Z.

A. Falvard, P. Henrard, D. Pallin, P. Perret and F. Saadi

Laboratoire de Physique Corpusculaire de Clermont-Ferrand
IN2P3/CNRS - Université Blaise Pascal
63177 Aubière Cedex France

Abstract

Final results of the global lepton analysis done with '90 and '91 data are presented:

$$\begin{aligned}
\Gamma(Z \to b\bar{b})/\Gamma(Z \to had.) &= 0.217 \pm 0.006 \pm 0.004 \\
\Gamma(Z \to c\bar{c})/\Gamma(Z \to had.) &= 0.174 \pm 0.005 \pm 0.016 \\
BR(b \to l) &= 0.116 \pm 0.003 \pm 0.004 \\
BR(b \to c \to l) &= 0.081 \pm 0.003 \pm 0.008 \\
< x_b > &= 0.712 \pm 0.004 \pm 0.011 \\
< x_c > &= 0.508 \pm 0.083 \pm 0.060 \\
\chi &= 0.115 \pm 0.014 \pm 0.007 \\
A^b_{FB} &= 0.088 \pm 0.012 \pm 0.002 \\
A^c_{FB} &= 0.100 \pm 0.020 \pm 0.017
\end{aligned}$$

This is a simultaneous measurement of $Z \to b\bar{b}$, $c\bar{c}$, $BR(b \to l)$, $BR(b \to c \to l)$, $B\bar{B}$ mixing, b and c fragmentation and asymmetry. This note also contains a short description of electron identification in the ECAL.

1 Introduction

This paper presents the final results obtained by the global lepton analysis about the measurements of $Z \rightarrow b\bar{b}$, $c\bar{c}$ couplings (Partial widths and asymmetries) and related parameters. Before the presentation of the analysis, a short presentation of electron identification with the ECAL is given. This is not a detailed description and it only intends to describe the methods used for identification and for the control of performances on the data themselves. Informations relevant for this analysis about muon identification have to be looked for in the parent paper written by our italian colleagues [1]. The selection of events, common to all the electroweak lepton analyses, can be found in a short Aleph note [2].

The presentation of the analysis is in two parts. First we present an analysis of the single lepton sample dedicated to the control of the quality of the analysis. In particular, high statistical accuracy measurements are obtained separately for electrons and muons to control that no significant differences exist for the two kind of leptons; this is useful since systematical effects are expected to be different for electrons and muons. Another aspect is to test with precise measurement of $BR(b \rightarrow l)$ that no significant dependance of our result with respect to the lepton p_t exists. In a second part, final results of the global analysis are presented and discussed.

2 Electron Identification

Electron-id is done by dE/dx measurement in the TPC and analysis of the shape of showers in the ECAL. These are independant determinations of the nature of the track in a large angular coverage of the apparatus. The general philosophy is to transform the basic informations (ionisation in the TPC, pattern and energy deposition in the ECAL storeys) into estimators which are numbers normally distributed on which a cut is applied to select electron candidates. The redundancies of TPC and ECAL informations allow to determine the performance of each estimator directly on data.

2.1 Electron-id in the ECAL

Both compactness of electromagnetic energy deposition around the original electron direction and the shape of energy deposition along the track are exploited.

2.1.1 R_T : an estimator of the electromagnetic shower compactness

Each charged track is extrapolated from the end of the TPC along a straight line and a crossing point is computed in each of the 3 stacks of the ECAL. This allows to determine in each stack the 4 storeys closest to the extrapolated track. This has to be adapted in some regions of the ECAL and more specifically

in the End-Cap when the size of a storey doesn't vary continuously in order to introduce no discontinuity in the performances: this can be satisfactory achieved in general and we will come back later on the particular problem of the overlap region where the electromagnetic shower develops in both the ECAL Barrel and End-Cap component. If E_i^j $(i = 1,4;\ j = 1,3)$ is the energy deposited in the i^{th} storey of the j^{th} stack, an electron estimator R_T is built for each charged track:

$$R_T = \frac{E_4/p \ - \ M}{\sigma_{E_4/p}}$$

where:

- M is the mean energy fraction deposited by an electron in the 4 centered towers. Its value is constant with the momentum, and is equal to 0.85 in the barrel region; in the end-caps this fraction increase to 0.89 due to a geometrical focusing effect induced by the magnetic field.
- $E_4 = \sum_{i,j} E_i^j$,
- p is the momentum of the charged track measured in the TPC,
- $\sigma_{E_4/p}$ is the resolution expected on the ratio; the resolution of the ECAL is dominant up to 25 GeV/c which is the range of interest for the present study.

The R_T estimator is more and more efficient to reject hadrons when the momentum of the track increases. In fact, even if a hadron doesn't have strong interaction in the ECAL, the average energy deposition of a minimum ionizing particle in the ECAL is of the order of 0.3 GeV, concentrated in the towers centered along the trajectory.

For low momentum tracks, the deposited energy has to be corrected, mainly for the zero suppresion effect and leackage. This becomes negligible for energies larger than 3 GeV/c which is the range used for the present analysis. For smaller energies, the variation of the average value of E_4/p with p was studied with $\gamma\gamma \rightarrow e^+e^-$ events and taken into account in the computation of R_T. Let us notice that the rear leakage effects are always very small whatever the energy is. For completeness they are computed and taken into account to compute R_T. Small residual effects can remain due to the absolute ECAL calibration which is done at the level of 1%. But at the end, efficiency and hadron rejection rate are determined directly on data by using the redundancies of electron-id in the ECAL and the TPC so that the absolute calibration is not a fundamental point for this analysis. What we care is that the sources for possible angular dependance are under control.

2.1.2 R_L : an estimator based on depth of energy deposition

The shape of energy deposition induced by an electromagnetic shower is classically decribed by:

$$f(t) = \frac{1}{E_0}\frac{dE}{dt} = (1 - \frac{b}{\beta})\frac{\beta^\alpha}{\Gamma(\alpha)}t^{\alpha-1}e^{-\beta t} \; + \; be^{-\beta t}$$

t is the depth in radiation length unit and E_0 is the total energy of the particle. $\Gamma(\alpha)$ is the Euler function to normalise $f(t)$. Among the three parameters, b is the ionisation component. It is equal to $0.018/E_0$ GeV^{-1}; its influence in the forthcoming analysis could only be non negligible for E_0 smaller than 0.5 GeV and so will be neglected everywhere.

The electron-id relies on the study of order 1 and 2 momenta of the longitudinal energy distribution $f(t)$. Neglecting the ionisation term, one gets the n-order momentum of $f(t)$ by:

$$< t^n >= \int_0^\infty f(t)t^n \; dt = \frac{\Gamma(\alpha+n)}{\beta^{\alpha+n}}\frac{\beta^\alpha}{\Gamma(\alpha)}$$

which looks very simple for 1- and 2-order momenta:

$$< t >= \frac{\alpha}{\beta} \quad ; \quad < t^2 >= \frac{\alpha(\alpha+1)}{\beta^2}$$

Let's mention that the total thickness of the ECAL, 22 X_0, is a sufficient approximation of infinity to compute the integrals for the present study. Experimentally the longitudinal profile of the shower can be measured through the energies deposited in the three stacks. From these three informations one is the total energy already used to compute the R_T estimator. Then two additionnal estimators can in principle be used. Analysis on the full shower done by using test beams at electron energies varying from 10 to 50 GeV has shown that β/α and $1/\alpha$ are independant variables with gaussian distributions [4]. This was confirmed at lower energies with the EGS4 Simulation. These variables are given by:

$$\frac{\beta}{\alpha} = \frac{1}{< s >} \quad ; \quad \frac{1}{\alpha} = \frac{< s^2 > - < s >^2}{< s >^2}$$

where $< s >$ is the average depth of energy deposition.
In real data $< s >$ and $< s^2 >$ are computed by using an iterative procedure. To start, we assume the incoming track to be an electron and the electromagnetic shower to have the average longitudinal profile corresponding to the incident energy measured by the TPC. Then the average position of the shower in each stack $< s_i >_{i=1,3}$ can be computed, just as $< s_i^2 >$. Then a first approximation of α and β for this shower can be computed and used for the second iteration. This converges very quickly. When the energy of the electron becomes too small, the large statistical fluctuation of the energy deposited in each stack can prevent the process to converge. This is fortunately not the case for electrons with energy

larger than 3 GeV. The way this procedure rejects hadron is in fact that most of the time hadronic showers cannot fit the shape of an electromagnetic shower; then the process is essentially divergent for hadron and convergent for electrons. While two independant estimators can be build, using the longitudinal profile of the shower, only one helps to remove hadrons when convergence is obtained. In fact the estimators are independant for true electrons but not for hadrons. Then the R_L estimator is defined by:

$$R_L = (\beta/\alpha - < \beta/\alpha >)/\sigma(\beta/\alpha)$$

The longitudinal profile information is computed on the truncated shower containing only the 2×2 storeys in each stack selected to compute R_T. This is to minimize the influence of a possible overlap of two clusters produced by two different charged or neutral particles. This slightly affects the parametrisation of $< \beta/\alpha >$ w.r.t. the shape of a full isolated shower. This one is done independantly for data and Monte-Carlo by using electrons selected by the R_T and ionisation estimators in hadronic events; electrons originating from Bhabha process are also used since the longitudinal profile of 45 GeV electrons has a small statistical fluctuation and so is a very good constraint.

Test beam studies have shown that the β/α parameter computed from the 3 stacks energies is independant of the angle of the incoming particle. A complementary study has been done by computing the same parameter from the 45 wire planes; it has shown that a sampling in 3 stacks is sufficient to define properly the shower profile.

2.1.3 Electron identification in the Overlap.

The overlap of the ECAL is the region where a photon coming from the center of the apparatus develops a shower in both the ECAL Barrel and End-cap. This is 4.2% of the angular coverage of the ECAL. While the towers remain projective in this region which make the previous analysis conceptually correct, there are two problems specific to this region;

- Loss of energy in the dead region between the Barrel and Endcap. This loss is not trivial and also affects the shape of the shower.
- leakage through the rear due to the smallest total thickness of the ECAL present in front of the particle $\simeq$ 16 X_0.

The analysis of the overlap region is quite complex. It has to take into account that:

- The total amount of material "seen" by an electron varies with ϕ.
- Losses are θ dependant, the dead region being not at the same depth with respect to θ
- Losses vary with particle momentum.

Essentially this is taken into account by two correction factors:

- C^0 for dead region losses: $C^0 = f_1(\rho, \phi)$
- C^l for leakage through the rear: $C^l = f_2(\theta, \phi)$

where ρ is the fraction of the shower energy found in the barrel. The function f_1 and f_2 have been parametrized [3] from test beam data. In front of each tower in the barrel, one finds a tower in the end cap which allows to define a "supertower". The energy in each supertower is corrected using the parametrization of f_1 and f_2 and the corrected energies are used to compute R_T and R_L. To do that correctly, the loss in the dead region is put in the first stack of the endcap and the rear loss in the last one which is assumed to go to infinity.

2.1.4 Cuts for e-id.

For the present analysis we favour a large rejection of hadron misidentification. This is to the expense of a lower efficiency. The following cuts are done on the two ECAL estimators:

$$-1.8 < R_L < 3.0 \quad ; \quad -1.6 < R_T < 999.$$

Figures 1 and 2 show in two plots the distribution of R_T versus R_L and what are the relative effects of the 3 estimators (R_T, R_L and R_I). The sample of tracks used in these figures is composed almost 50%-50% by electrons and hadrons.

Let's remark that no higher cut is applied on the estimator related to the compactness of the shower. This is due to the fact that the 4 central towers associated to an electron can contain additionnal energy from a bremsstrahlung photon. Then an upper cut on R_T would kill true electrons and would not help significantly for hadron rejection.

2.1.5 Efficiency of the e-id by the ECAL.

The pairs produced by the photon materialisation in the beam pipe, Vertex Detector, ITC and inner wall of the TPC is a natural and pure source of electrons used to measure the efficiency of e-id.

All the charged tracks are associated to each track with an opposite electric charge to find a pair coming from $\gamma \rightarrow e^+e^-$. This is done using the QPAIRFD package looking at the distance between the reconstructed trajectories of the two particles in the (r, θ) and (r, ϕ) plane computed at the estimated materialisation point: both distances are required to be smaller than 1cm. Finally the mass of the pair assuming electron masses for both particles has to be smaller than 20 MeV/c^2. This sample remains contaminated by hadronic V^0's. This can be shown on Fig. 3 giving the materialisation radius of the selected pairs. Several procedures are used to produce an enriched sample of electrons.

- One looks at one track of the V^0 by tagging the electron type of the other one by ECAL e-id and dE/dx when available.

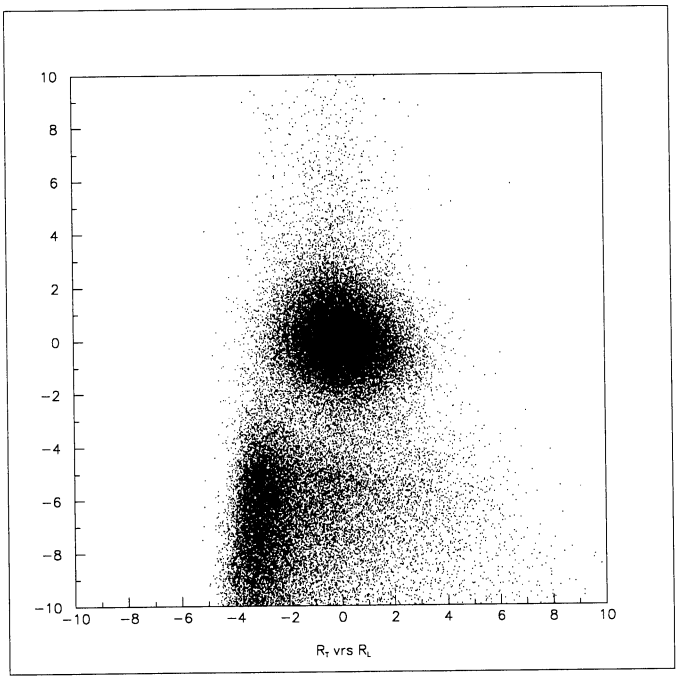

Figure 1: R_T versus R_L without R_I cut

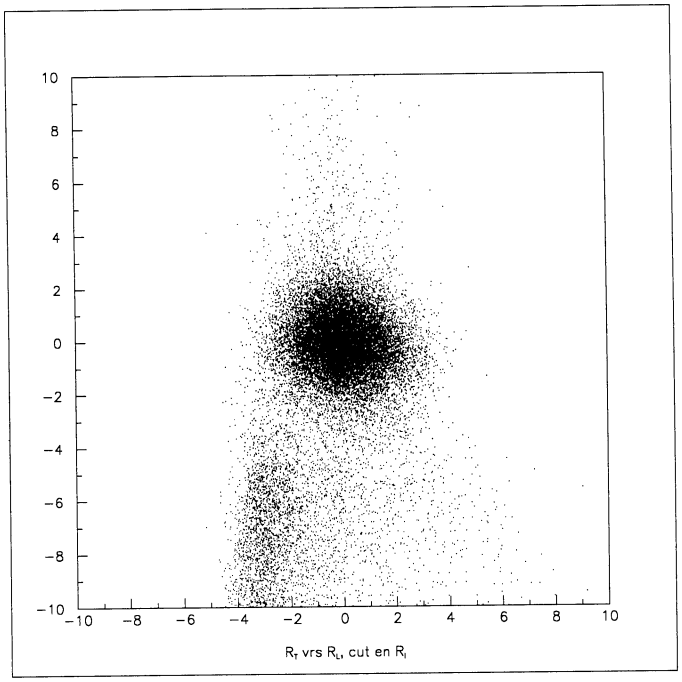

Figure 2: R_T versus R_L with R_I cut (R_I > - 2.5).

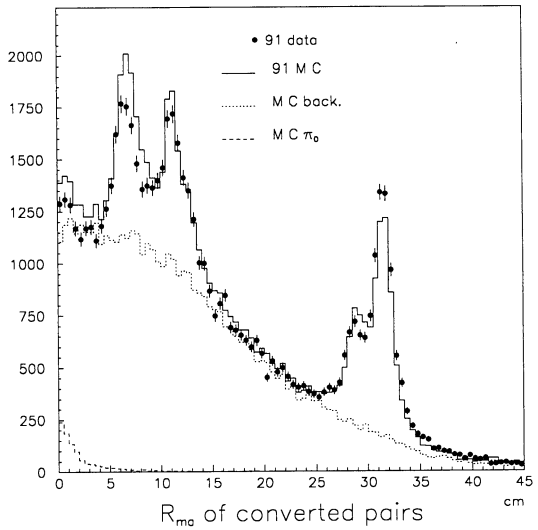

Figure 3: Materialisation radius of all the pairs wih $M_{e^+e^-} < 20$ MeV

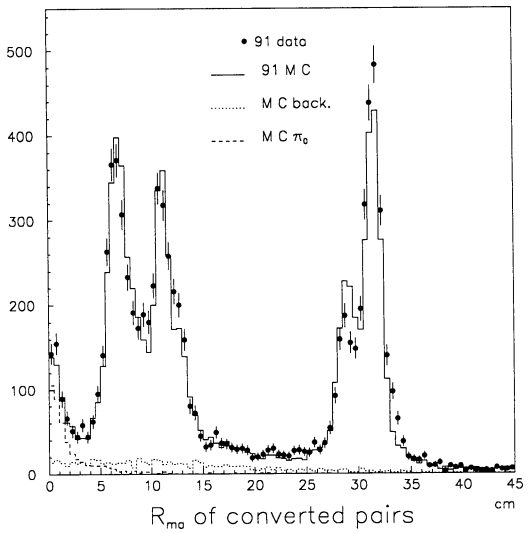

Figure 4: Materialisation radius of V^0 with one electron candidate

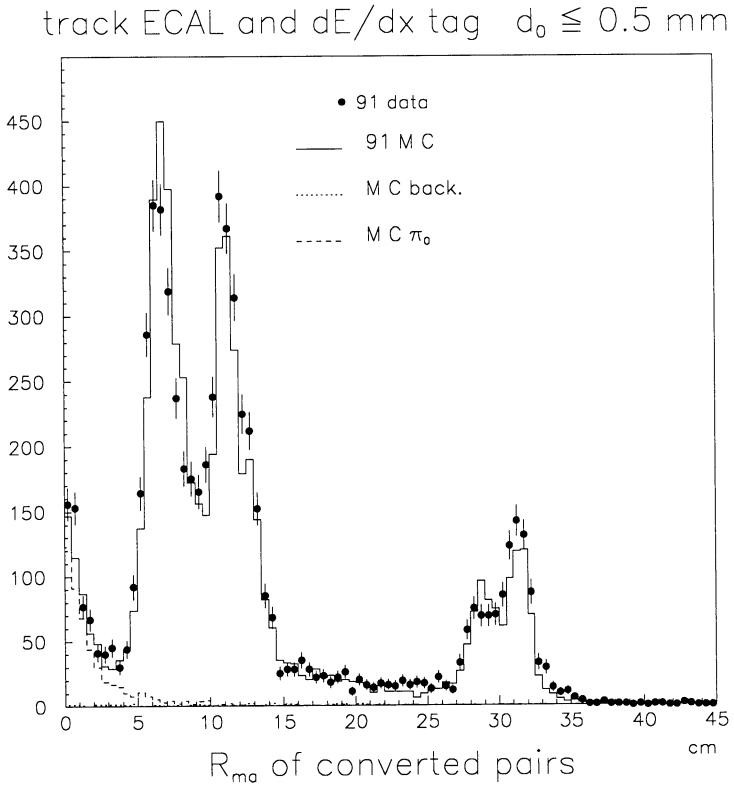

Figure 5: Comparison of materialisation rates in DATA and MC after identification. $Data^{91}/MC = 1.052 \pm 0.016$

Both tracks are required to have momenta larger than 3 GeV/c. Selecting the tracks originating from the Vdet/Inner wall of the ITC (6.0 cm $< R_{mat} <$ 14.0 cm) and Outer wall of the ITC/Inner wall of the TPC (28.0 cm $< R_{mat} <$ 33.5 cm, Fig. 4) we get a sample enriched at 98% in electrons.

• One looks at each track in the pairs previously defined without any constraint on its partner. The electron sample is enriched by imposing a hard cut on the dE/dx ($R_I >$ -0.5). Only tracks originating from the ITC Outer wall and TPC Inner wall are selected providing a 98% electron sample.

Tracks which succeed the two procedures are taken once. This provides a sample of electrons 98% pure. Then efficiency of the identification by the ECAL can be measured for Data and Simulated events separately w.r.t. p, p_t and θ of the track; this is summarized in tables 1, 2 and 3 for data.

$\cos\theta$	0. - 0.2	0.2 - 0.4	0.4 - 0.6	0.6 - 0.8	0.8 - 1.
ϵ^e	0.82 $\pm$ 0.017	0.86 $\pm$ 0.015	0.84 $\pm$ 0.013	0.76 $\pm$ 0.013	0.75 $\pm$ 0.013

Table 1: Angular efficiency of the ECAL for e-id

p_t	0. - 0.25	0.25 - 0.5	0.5 - 0.75	0.75 - 1.	$>$ 1.
ϵ^e	0.78 $\pm$0.011	0.79 $\pm$ 0.011	0.80 $\pm$ 0.017	0.79 $\pm$ 0.028	0.78 $\pm$ 0.03

Table 2: Efficiency of the ECAL for e-id w.r.t. the electron p_t

p	3. - 5.	5. - 8.	$>$ 8.
ϵ^e	0.79 $\pm$ 0.01	0.79 $\pm$ 0.013	0.76 $\pm$ 0.02

Table 3: Efficiency of the ECAL for e-id w.r.t. the electron momentum

The efficiency for e-id in the ECAL looks almost independant of p and p_t. The smallest efficiency in the large $cos\theta$ region is due to the larger fraction of cracks in this region of the ECAL. The same measurements are done for Data and Simulated events. Then in the forthcoming analyses, the efficiency measured on data is used. Table 4 and 5 give the ratio of efficiencies measured for data and MC events. Fig. 6 shows the absolute efficiency of the e-id in the ECAL in the 4 bins of tables 4 and 5.

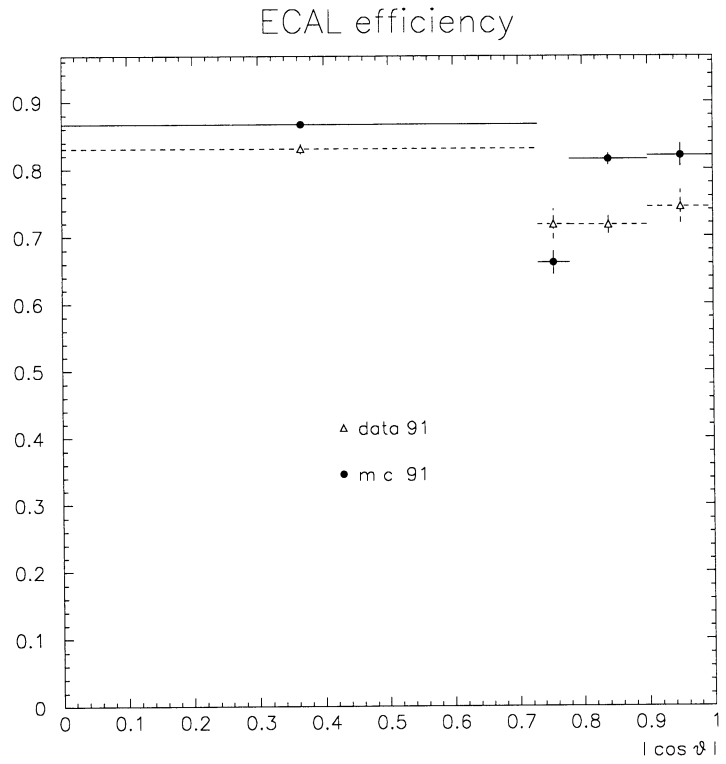

Figure 6: Efficiency of e-id in the ECAL for Data and Monte-Carlo. The 4 bins are used in the analysis: Barrel, Overlap and two bins in the End caps.

	$cos\theta < 0.73$	$cos\theta < 0.78$	$cos\theta < 0.90$	$cos\theta < 1.00$
$P_t < 0.25$	0.956 ± 0.026	1.210 ± 0.138	0.856 ± 0.042	0.901 ± 0.095
$P_t > 0.25$	1.000 ± 0.020	1.010 ± 0.086	0.828 ± 0.035	0.726 ± 0.074

Table 4: Efficiency corrections DATA / MC for the ECAL in 1990

	$cos\theta < 0.73$	$cos\theta < 0.78$	$cos\theta < 0.90$	$cos\theta < 1.00$
$P_t < 0.25$	0.938 ± 0.016	0.972 ± 0.070	0.894 ± 0.031	0.945 ± 0.056
$P_t > 0.25$	0.969 ± 0.012	1.150 ± 0.056	0.873 ± 0.023	0.880 ± 0.046

Table 5: Efficiency corrections DATA / MC for the ECAL in 1991

2.1.6 Purity of the electron sample selected by the ECAL

The purity of the electron sample selected with the ECAL is controled by looking at the dE/dX information of the selected tracks. Then the control is only correct for tracks which have a dE/dx information. In particular requiring that the particle has at least 50 dE/dX measurements not shared by another track makes the situation better for higher-p_T particles. In this analysis, we always require that both ECAL and dE/dx measurements are available so that the procedure is valid.

Fig. 7-a shows the R_I distribution for ECAL electron candidates in some p, p_t range ($5 < p < 8$ GeV/c, $p_t < 0.25$ GeV/c). The normal gaussian from electrons is dominant but the residual hadronic contamination is not negligible. The shape of hadronic events can in first approximation be evaluated from non-electron candidates ($RT < -1.6$, $R_L < -1.8$). This procedure is in principle not perfect since the cross sections of π, K, p and $\bar{p}$ in the materials are significantly different. Then the probability that a track is identified as electron in the ECAL is different for each type of particule. Then the overall dE/dx shape is a priori different for hadrons selected as electron or non-electron candidates. To estimate the hadronic contamination we proceed along the following way. Starting with a R_I distribution of the electron candidates in some (p, p_t) region, we fit it by the function:

$$N^e f^e(R_I) + N^h f^h(R_I)$$

where N^e and N^h are the numbers of electrons and hadrons present in the sample, f^e and f^h being the shapes of electrons and hadron R_I distributions. f^e is simply assumed to be a gaussian with free average and sigma. As an approximation, f_h is taken to be similar to the distribution of tracks non selected as electrons in the ECAL; in fact a more severe criterium is choosen in order to remove all the

electrons ($R_T, R_L < -2.3$). Then the gaussian of true electrons is subtracted and we remain with the hadronic contamination (Fig. 7-b).

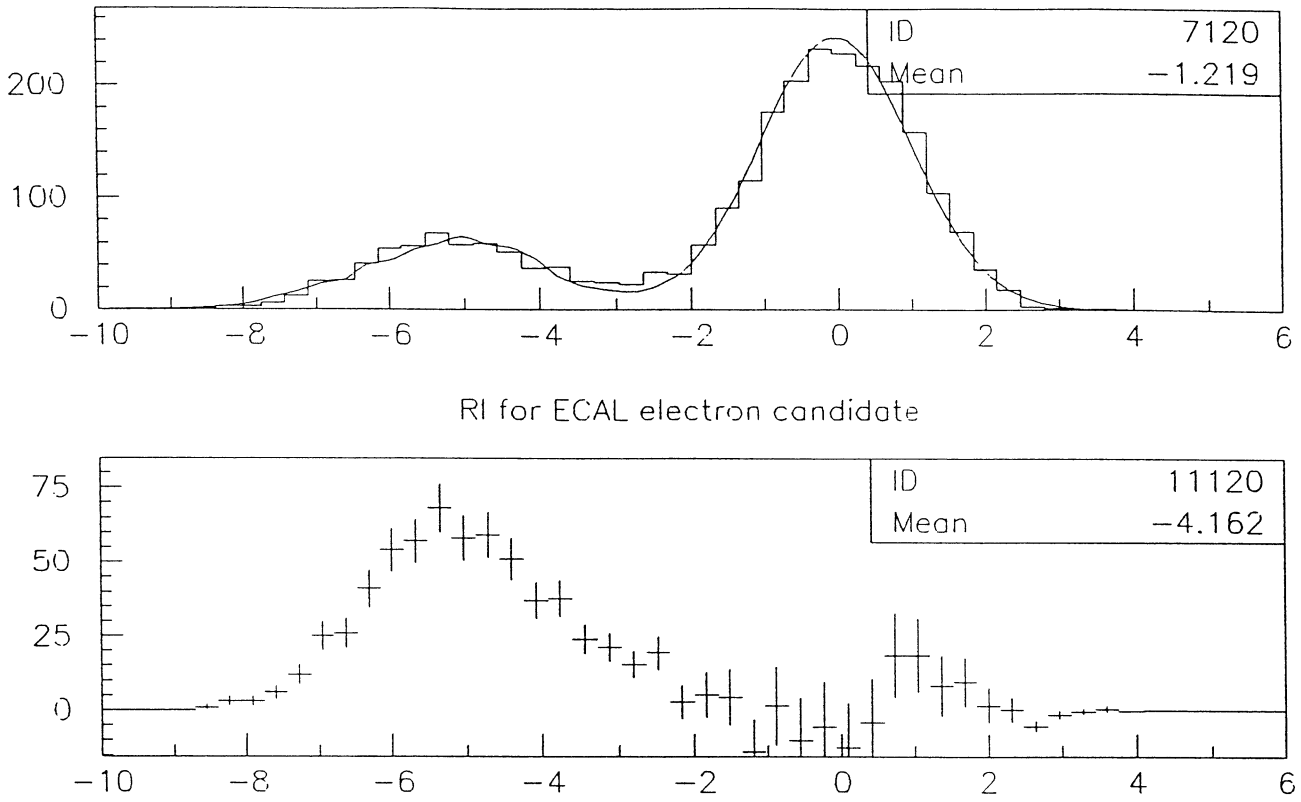

Figure 7: R_I distribution for ECAL e candidates.

This is done for Data and Monte Carlo. The difference between data and Monte-carlo is estimated in the range $-3.5 < R_I < -1.5$ and applied to the full range $-2.5 < R_I$; it was shown with Monte-carlo events (Fig. 10) that this estimate of the hadron contamination is correct.

3 Electron-id in the TPC

For details we refer to TPC experts. We only present the aspects which are relevant for this study. The R_I estimator is computed from the dE/dx as soon as at least 50 wires have a measurement for the track without any overlapping particle. Then a cut ($R_I > -2.5$) is done. In fact the 50 wires cut is the main problem which has to be controlled since the efficiency of this cut is not well reproduced by the Monte-Carlo. The difference between data and Monte-carlo can be measured with a very high accuracy by looking at the efficiency of the cut for all tracks(Fig. 8 and 9). Let us mention that this difference depends on θ, p and p_t and this variation is taken into account in the forthcoming analysis.

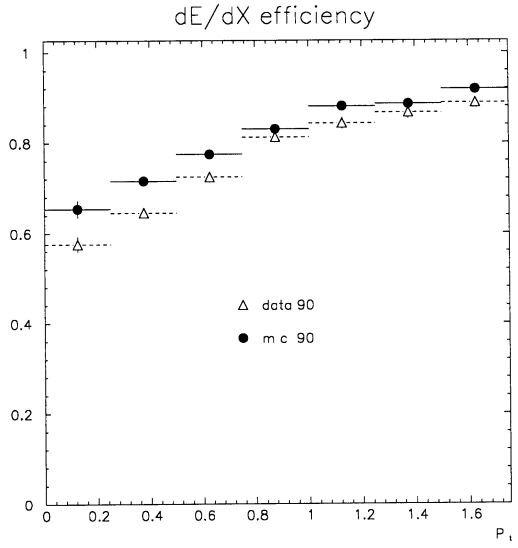

Figure 8: Variation of the dE / dx efficiency with P_t in 1990 for the data and MC

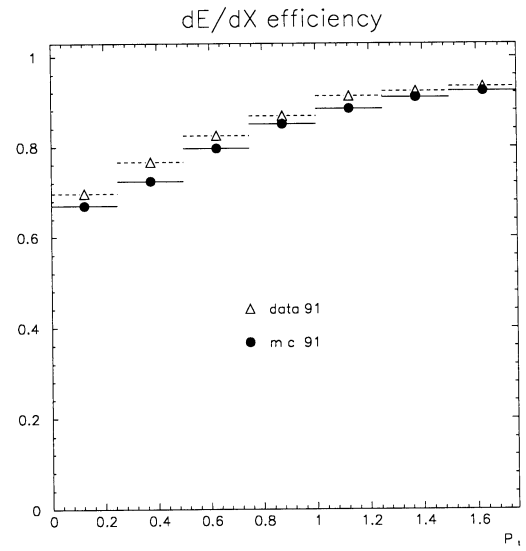

Figure 9: Variation of the dE / dx efficiency with P_t in 1991 for the data and MC.

Fig. 10 shows the probability that a hadron is identified as an electron by the ECAL alone. It is clear on these figures that hadron rejection is very good in the electron channel. Even with ECAL alone a probability of hadron misid is of the order of a few per mill.

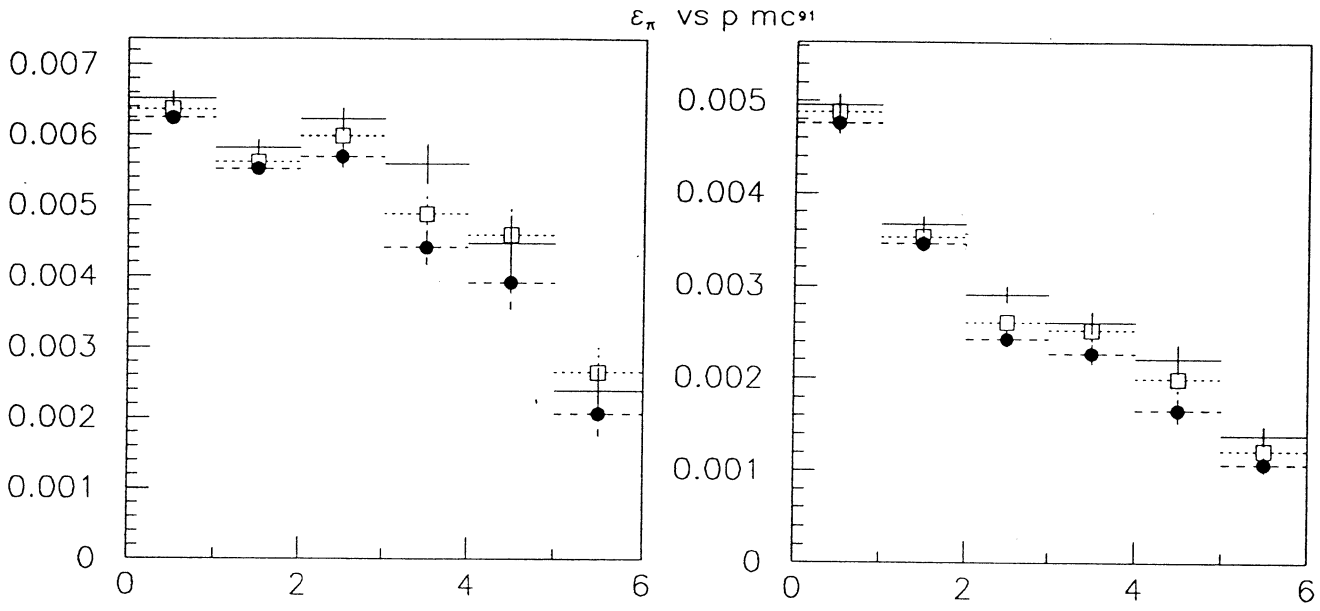

Figure 10: Probability of hadron misid in the ECAL- Momentum bins are: 2-3, 3-5, 5-8, 8-11, 11-14, >14. The two figures are for $p_t < 0.5$ GeV/c (Left) and $p_t > 0.5$ GeV/c (Right). The crosses are for history, the squared for reconstruct MC events and the dots can be ignored.

4 The ALEPH Monte-Carlo for $Z \rightarrow q\bar{q}$ events simulation.

The Monte-Carlo program used in ALEPH for the present study, named HVFL02, is based on JETSET7.3 [5]. Several modifications or additions have been done in order to make possible or more flexible the implementation of various physics options or change. Let us mention that some developments were done for the previous version of JETSET and are maintained for coherence: this is mainly the case for $B\bar{B}$ Mixing, including time evolution. Let us list below the main modifications applied to the standard JETSET 7.3 code.

- The process $e^+e^- \rightarrow q\bar{q}$ is generated by using the DYMU02 code [6] to improve the initial state radiation. Final state radiation of photons and gluons is done in the JETSET 7.3 scheme.
- The decay channels of charmed hadrons take into account the last experimental results for both exclusive and inclusive modes.
- Two body branching ratios of the B hadrons measured by ARGUS and CLEO are used. Non measured two body decays are computed from the measured ones using the Stech-Bauer approach[7].
- Baryonic B mesons decays don't exist in JETSET and are implemented to reproduce the measurements of inclusive production[8].
- In JETSET the simulation of $B \rightarrow J/\psi + X$ decays is done through a mechanism which produces only two body final states. This doesn't reflect the experimental observations. So the decay chain was modified to produce multibody B decays including J/ψ and the agreement with data is satisfactory. The ψ' production from B mesons is also added with a correct simulation of the $\psi' \rightarrow \psi\pi\pi$ decay [9].
- The $B \rightarrow l\,\bar{\nu}_l\,D$ and $B \rightarrow l\bar{\nu}_l D^*$ dynamics has been modified. Three models are implemented [10]. As a standard for MC productions the Korner-Schuler model is choosen. Higher mass contributions $B \rightarrow l\,\bar{\nu}_l\,D^{**}$ and $B \rightarrow l\bar{\nu}_l D^*\pi$ are also included with an amplitude "a la JETSET"; the branching fraction of B to such higher mass states is taken to reproduce the fit of the lepton energy spectrum done "a la Altarelli" by ARGUS and CLEO [11]. Let us mention that in the forthcoming analysis the generated events are weighted a posteriori to simulate all suitable modelisations according to the event by event lepton energy in the B rest frame.
- The $b \rightarrow u$ transition is introduced in HVFL02 with a total branching fraction of 3%. The free quark model is assumed and each inclusive decay mode is introduced with a rate computed with phase space [12]. The fraction of exclusive $B \rightarrow l\bar{\nu}_l(\pi$ or $\rho)$ can be modified by a local change of a JETSET parameter. In our standard production these two decay modes correspond to approximately 60% of all the semileptonic

decay modes; this corresponds to the standard JETSET but is quite large with respect to several theoretical predictions [13]. Other more sophisticated options are also possible in the program but are not used for production.

5 Analysis of the Inclusive Lepton Production.

The analysis of the (p, p_t) distribution of all the lepton candidates in the hadronic Z decays was commonly used to measure simultaneously $BR(b \rightarrow l)\Gamma_b/\Gamma_h$, $BR(c \rightarrow l)\Gamma_c/\Gamma_h$, b and c fragmentations and asymetries. This kind of analysis permits to get the measured parameters, especially $BR(b \rightarrow l)\Gamma_b/\Gamma_h$, with an high statistical accuracy and will be mainly used to look at possible remaining systematical problems. This is of specific interest to compare results obtained with electrons and muons separately or to control p_t dependance of the result which could reflect some significant misunderstanding in this high accuracy analysis.

In practice, this section presents an improvement of this method to include a measurement of $BR(b \rightarrow c \rightarrow l)$. This is done by analysing events with two lepton candidates with opposite electric charges in the same hemisphere. This sample contains a large fraction of dileptons originating from $(b \rightarrow l\bar{\nu}_l + (c \rightarrow \bar{l}\nu + (s \ or \ d)))$ which makes the number of events closely dependant of $BR(b \rightarrow l)\ BR(b \rightarrow c \rightarrow l)\ \Gamma_b/\Gamma_h$. More precisely the same hemisphere dileptons are analysed in the plane $(p_{\otimes}, p_{tmin})$ optimising the separation of $b\bar{b}$ events w.r.t. lighter quarks; these two variables are defined from the basic transverse and longitudinal components p_t and p_l of the lepton momentum w.r.t. the jet direction:

$$p_{\otimes} = p_{t1}p_{l2} + p_{t2}p_{l1} \quad ; \quad p_{tmin} = Min(p_{t1}, p_{t2})$$

Except this $(b \rightarrow l^-l^+ + X)$ component the sample contains residual backgrounds with a lepton from misidentification or light quark decays associated to a lepton from heavy quark: $b \rightarrow l$, $b \rightarrow (c \ or \ \bar{c} \rightarrow l)$, $c \rightarrow l$. In the likelihood to be maximized, these residual contributions are set proportionnal to the values of $BR(b \rightarrow l)$, $BR(b \rightarrow (c \ or \ \bar{c} \rightarrow l))$, $BR(c \rightarrow l)$ of the fit.

In this analysis we are not interested to measurements sensitive to the electroweak SM which will be developped in the forthcoming section: then Γ_b/Γ_h and Γ_c/Γ_h are fixed to there values from the Standard Model assuming $m_t = 150\ GeV/c^2$. A rough description of the mechanics of the fit can be given:

- High p_t leptons give the value of $\Gamma_b/\Gamma_h\ BR(b \rightarrow l)$
- Same hemisphere opposite charge dileptons give $\Gamma_b/\Gamma_h\ BR(b \rightarrow l) \times BR(b \rightarrow c \rightarrow l)$. As $\Gamma_b/\Gamma_h\ BR(b \rightarrow l)$ is known with a large accuracy from single leptons, this provides the measurement of $BR(b \rightarrow c \rightarrow l)$.
- Low p_t leptons originate dominantly from $c \rightarrow l$, $b \rightarrow (c \ or \ \bar{c} \rightarrow l)$ and residual backgrounds. The $b \rightarrow c \rightarrow l$ contribution is known from

same hemisphere opposite charge dileptons. $b \rightarrow \bar{c} \rightarrow l$ is expected to be one order of magnitude smaller than $b \rightarrow c \rightarrow l$ and is taken from the simulation. Then $\Gamma_c/\Gamma_h \; BR(c \rightarrow l)$ can be measured with an accuracy which is essentially limited by the uncertainty on background from misidentification and light quark decays.

We have mentionned the sources of informations where the branching ratios can be extracted. But the analysis takes into account the shape of the various contributions in the planes (p, p_t), $(p_\otimes, p_{tmin})$. This is at the beginning taken from Monte-Carlo. But this one is not perfect in several aspects and has to be corrected at the time where the analysis is done.

- Internal bremsstrahlung in the b and c semileptonic decays $(b, c \rightarrow l\gamma + X)$ is not introduced in the Monte-Carlo. Several theoretical approachs describe this process[14] [15]. Using PHOTOS the ratio of the lepton energy spectra with and without internal bremstrahlung has been parametrized[16] as a function of the energy of the lepton in the b or c hadron rest frame. When analysing simulated events, the lepton energy in the b or c hadron rest frame is stored and during the fit each Monte-Carlo event is weighted using this parametrisation. This treatment gives an approximation of the correction. In fact only the lepton energy is corrected and not its direction which can be affected by photon radiation. Nevertheless this should be a sufficient approximation since the main effect is to correct $BR(b \rightarrow e)$ by 4%. For future analysis (data '92) the PHOTOS package is used in HVFL03 to fully simulate the internal bremsstrahlung.

- Another problem of the lepton analysis is related to the shape of the lepton energy spectrum in the b hadron rest frame. There is a quite large agreement to describe the $B \rightarrow l\bar{\nu}(D \; or \; D^*)$ decays since all the models presently available give similar prediction. But the influence of higher mass charmed states remain presently badly known. A first approach is to treat the problem of $B \rightarrow l\bar{\nu} + X$ decays in an inclusive way by using the Altarelli et al. description [17]. At the level of the generator this is done by adding exclusive channels $B \rightarrow l\bar{\nu}D^{**}$ and $B \rightarrow l\bar{\nu}D^*\pi$ with a branching fraction choosen to reproduce the shape of the lepton energy spectrum fitted by ARGUS and CLEO experiment. This gives a shape for the (p,p_t) distribution of the leptons in the laboratory (let us mention that at this stage the Altarelli parametrization from ARGUS and CLEO is corrected for internal Bremsstrahlung). Another approach is to include explicitely higher mass states through various D^{**} states according to the model of Grinstein, Isgur, Scora and Wise [10]. This was done by both ARGUS and CLEO collaborations. The fraction of D^{**} which has to be added to D and D^* is in the range (30-40)% dependent on the kind of analysis. Such a large fraction of D^{**} corresponds to a lepton energy softer than the one obtained from the best fit with an Altarelli distribution. Technically it is trivial to

change the model in our analysis. In fact the full Monte-Carlo events are simulated with some model: this leads to a lepton energy spectrum in the b rest frame, $LS_{ini}(E^*)$. If we want to simulate another lepton energy (E^*) spectrum in the b rest frame with some $LS_{ana}(E^*)$ spectrum we simply have to weight each simulated event by $LS_{ana}(E^*)/LS_{ini}(E^*)$.

• Another important modification has to be implemented. This is the effect of fragmentation simulation for heavy quark. In fact in the standard HVFL02 program, the b and c fragmentation are simulated using the so-called *Peterson* model [18]. The parametrization in this model is only dependant on one parameter for each quark flavour commonly noticed ϵ_c and ϵ_b. Two problems can occur:

- During the fit we look for the value of ϵ_b and ϵ_c optimizing the shape of the lepton energy spectrum to describe the data.

- While the Peterson parametrisation is very popular to describe heavy quark fragmentation, it is useful to look for the sensitivity of our results to a change of model to describe this fragmentation.

To treat correctly these problems we store for each generated event the generated value of z (to a first approximation z is the fraction of the heavy quark quadri-momentum transfered to the heavy hadron) for each quark. Then if $Frag_{ini}(z)$ is the z distribution function at the time of the generation and $Frag_{ana}(z)$ the z distribution function to do the analysis we simply weight the generated events by $Frag_{ana}(z)$ $/Frag_{ini}(z)$. $Frag_{ana}(z)$ can change at each step of the fit if we look for the optimum ϵ_Q.

5.1 Results

In this analysis all the corrective factors for efficiencies and purities mentionned in the parts describing electron and muon identification have been introduced.

Table 6 gives the results obtained for electron and muon separately with the analysis described previously. Here only statistical errors are shown. Within errors the agreement is quite good. The three first columns are obtained with the Altarelli parametrisation of CLEO/ARGUS (noticed Al) and the 4^{th} column with the GISW CLEO Parametrisation (noticed GI). Looking for the effect of $b \rightarrow l$ models we note the following:

for each parameter we take as our best result the average value obtained for the two models. This gives $BR(b \rightarrow l) = 0.116 \pm 0.003$ (syst. from model), $BR(b \rightarrow c \rightarrow l) = 0.0825 \pm 0.0055$ (syst. from model). The effect of modelisation is quite small especially for $BR(b \rightarrow l)$. This is partially due to the result for fragmentation. Going from Altarelli Model to GISW Model the lepton energy spectrum in the b rest frame becomes softer; this is compensated by a larger boost leading to an increase of

the best $< x_b >$. The table 7 shows in addition that '90 and '91 data give consistent results within statistical errors.

Parameter	e '90 + '91 (Stat. error)	μ '90 + '91 (Stat. error)	e+μ '90+'91 Al (Stat. error)	e+μ '90+'91 GI (Stat. error)
$BR(b \to l)(\%)$	11.1±0.2	11.3±0.2	11.3±0.1	11.9±0.1
$BR(b \to c \to l)(\%)$	8.9±0.5	8.8±0.4	8.8±0.2	7.7±0.2
$BR(c \to l)(\%)$	10.4±0.4	9.2±0.4	9.7±0.2	9.5±0.2
$< x_b >$	0.713±0.007	0.696±0.007	0.702±0.003	0.722±0.004
$< x_c >$	$0.54^{+0.012}_{-0.013}$	$0.503^{+0.012}_{-0.010}$	0.514±0.009	0.515±0.009

Table 6: Comparison of e and μ results in '90 + '91

Parameter	e+μ '90 GI (Stat. error)	e +μ'90 Al (Stat. error)	e +μ '91 Al (Stat. error)	e +μ '91 GI (Stat. error)
$BR(b \to l)(\%)$	12.1±0.2	11.4±0.2	11.2±0.1	11.8±0.1
$BR(b \to c \to l)(\%)$	8.0±0.4	9.2±0.4	8.5±0.3	7.4±0.3
$BR(c \to l)(\%)$	10.0±0.4	10.1±0.5	9.5±0.3	9.2±0.3
$< x_b >$	0.725±0.006	0.705±0.006	0.701±0.005	0.721±0.005
$< x_c >$	$0.479^{+0.019}_{-0.006}$	$0.48^{+0.052}_{-0.007}$	$0.534^{+0.011}_{-0.013}$	$0.54^{+0.011}_{-0.013}$

Table 7: Comparison of e + μ results in '90 and '91 for the 2 models

We use the highly accurate measurement of $BR(b \to l)$ to control if some distorsion of the result appears due to some misunderstanding of background or modelisation. This is done by looking at the variation with p_t of $BR(b \to l)$ and ϵ_b. In this study the other parameters which are extracted by using low p_t leptons ($BR(b \to c \to l)$, $BR(c \to l)$, ϵ_c) are set to there measured values with no p_t cut. Results are given in table 8: no significant p_t dependance is observed in the full range of interest. The study is done with '91 leptons since

$P_t >$	0.	0.5	0.75	1.0	1.25	1.5
$BR(b \to l)$	11.20±0.12	11.21±0.12	11.21±0.12	11.16±0.13	11.29±0.15	11.44±0.17
$< X_b > (\%_0)$	701±4	701±4	697±5	701±5	694±5	689± 7

Table 8: $BR(b \to l)$ with respect to p_t assuming Standard Model for Γ_b in the global fit '91 data e + μ .

the statistics for '90 MC is quite small and possible variation at large p_t could be induced by the small MC statistics and not reflect a real effect.

6 Global Analysis

6.1 Principles of the analysis

The informations contained in the events with at least 2 leptons (**Dilepton Sample**) are combined with the Single Lepton Sample to measure simultaneously the partial decay width of the Z^0 into $b\bar{b}$ and $c\bar{c}$, the branching ratio $(b \to l)$ and $(b \to c \to l)$. A propotype of such an analysis was given in the previous section where same hemisphere opposite side dileptons were used to measure $BR(b \to c \to l)$. Such a method allows to get the B-$\overline{\text{B}}$ mixing in a simultaneous measurement with the branching ratios $BR(b \to l)$ and $BR(b \to c \to l)$ to which it is strongly correlated. Standard procedures to extract b and c asymmetries, A_b and A_c, are also implemented; this permits to extract in a simultaneous analysis all the parameters relevant for the test of the electroweak standard model.
In opposition to the previous section which was essentially devoted to the test of our understanding of the various ingredients, we are interested in this part to extract parameters which are sensitive to the heavy quark couplings to the Z: $Z \to b\bar{b}$ and $Z \to c\bar{c}$ partial widths, A_b and A_c. In fact it is difficult and for the moment being not realistic to extract in a simultaneous analysis $\Gamma(Z \to c\bar{c})$ and $BR(c \to l)$. That's the reason why we have choosen to fix $BR(c \to l)$ to its world average: $BR(c \to l)$ =(9.8±0.5)%. Let's note that this value is in good agreement with our previous determination (see table 6).

6.2 The dilepton sample

From events containing at least two leptons, we build all the possible combinations of two leptons. This means that for an event with 3 lepton candidates, 3 combinations are used.
Two categories of dileptons are defined: the **same side dileptons** and **opposite side dileptons**. The classification was simply done by looking at the angle between the direction of the two leptons. If larger than 90^o the leptons are called *opposite side* and *same side* otherwise.

- **Opposite Side Dilepton Sample** :
  It contains the following contributions with a hierarchy respective to the number of high-$P_\perp$ leptons:
  - $(b \to l)(\bar{b} \to l)(Z \to b\bar{b})$
  - $(b \to l)(\bar{b} \to \bar{c} \to l)(Z \to b\bar{b})$
  - $(b \to c \to l)(\bar{b} \to \bar{c} \to l)(Z \to b\bar{b})$
  - $(c \to l)(\bar{c} \to l)(Z \to c\bar{c})$
  - Backgrounds. Very often this contains one "physical lepton" from b or c semileptonic decays.

By splitting this sample in same electric charge events and opposite electric charge events, informations about the B-$\overline{\text{B}}$ mixing is obtained.

- **Same Side Dilepton Sample:**
  As mentionned in the previous section, it is very usefull in this analysis since it originates mainly from one physical process: $b \rightarrow lepton + \nu_l + (c \rightarrow lepton + \nu_l + s \ or \ d)$. Other small contributions exist but come mainly from additionnal backgrounds: the specific case of $B \rightarrow J/\psi + X$ will be discussed in the next paragraph. The fraction of events with same electric charge dileptons are only from background in that sample. So only the opposite charge dileptons are kept in this sample.

6.3 Choice of the analysis variables

The problem is to use the kinematics to discriminate the $b \rightarrow l\bar{b} \rightarrow l$ contribution from all others. For each couple of leptons, the basic informations are $(p_{li}, p_{ti})_{i=1,2}$, p_{li} and p_{ti} being the longitudinal and transverse momenta of the lepton with respect to the closest jet. Then the problem is to find the most discriminant combinations of these basic variables. This was done in a general way by doing a F-test on all possible combinations to improve the discrimination of the $(b \rightarrow l)(\bar{b} \rightarrow l)$ class of events with respect to all other sources of dileptons. The classification of the best variables is shown in table 9 .

variable	F value	Correlation
$p_{t1}p_{l2} + p_{t2}p_{l1}$	713	1.00
$p_{t1} + p_{t2}$	700	0.74
$Max(p_{t1}p_{l2}, p_{t2}p_{l1})$	694	0.96
$p_{t1}p_{t2}$	612	0.75
$Min(p_{t1}, p_{t2})$	560	0.68

Table 9: F-test criterium for the most discriminant variables

The correlation given in the table refers to the correlation with respect to the most discriminant variable. We require quite arbitrarily that the correlation between two variables is smaller than 0.7 so that the first and fifth variables are used. Using the same notation as in the previous section, we note the first variable by $p_{\otimes}$ in the forthcoming pages while the 5^{th} variable is called p_{tmin}. This choice was already proposed by the MARK II collaboration in a slightly different form [19]. The first variable is very discriminant for the $(b \rightarrow l)(\bar{b} \rightarrow l)$ contribution since in this case p_{ti} and p_{li} are large for both leptons. The second variable is discriminant due to the large p_t distribution of the $b \rightarrow l$ contribution with respect to all the other sources of leptons. The procedure was systematics and all the results are not completely intuitive; when an optimisation is required,

it is difficult to justify a choice of discriminant variables without the help of such a numerical test based on performant statistical analysis.

Let us notice that the couple of variables ($p_{\otimes}$,p_{tmin}) can be defined for same side and opposite side dileptons. For the same side dileptons the goal is to discriminate the $b \to (l\bar{\nu}_l(c \to \bar{l}\nu_l s))$ source of leptons. Natural contaminations come from residual γ materialisation, Dalitz decays and $J/\psi \to l^+l^-$ decays. The J/ψ contribution provides leptons with high total and transverse momenta which are well controlled by there $p_{\otimes}$ and p_{tmin} distributions. So no additionnal cut was done to remove the lepton contribution from J/ψ decays. At the end, it was verified that the limited knowledge of $B \to J/\psi + X$ doesn't introduce a significant systematical error in the analysis. It is clear that the two variables optimized for the opposite side dileptons are not so interesting for same side dileptons. But it was shown that this is the best possible combination of p_{ti}, p_{li} to disentangle the $b \to (l\bar{\nu}_l(c \to \bar{l}\nu_l s))$ contribution.

6.4 Mechanics of the fit

While everything is done simultaneously, the results (see page 38) can be discussed as a multi-step mechanism:

- The single lepton sample provides severe constraints on the product $P_b = BR(b \to l)\gamma_b$ and $< x_b >$ ($< x_b >$ is the average fraction of the beam energy taken by b-hadrons); this is due to the dominant contribution of direct semileptonic b decays in the high-p_t region. The low p_t region constrains $BR(c \to l)\gamma_c$ and the $< x_c >$; the other low p_t physical contribution from $BR(b \to c \to l)\gamma_b$ is obtained from same side dileptons (see previous section). This sample is also split in 2 parts according to the cos θ angle of the event thrust axis to measure the A_{FB}^b and A_{FB}^c asymmetries for $b\bar{b}$ and $c\bar{c}$.
  The number of leptons in a (p, p_t) box is given by:

$$
\begin{aligned}
\mathrm{NS}(\mathrm{p}, \mathrm{p_t}, \theta) \;= (\;\; & 2\,\gamma_b \Big[(f_{b\to\ell}(p,p_t,\theta,\varepsilon_b) BR(b \to \ell) \\
& + f_{b\to\tau\to\ell}(p,p_t,\theta,\varepsilon_b) BR(b \to \tau \to \ell) \\
& + f_{b\to W\to(\bar{c}s)\to\bar{\ell}}(p,p_t,\theta,\varepsilon_b) BR(b \to W \to (\bar{c}s) \to \ell)) \, A_b(\theta) \\
& + f_{b\to c\to\ell}(p,p_t,\theta,\varepsilon_b)\, BR(b \to c \to \ell)\, A_b(-\theta) \Big] \\
& + 2\,\gamma_c\, f_{c\to\ell}(p,p_t,\theta,\varepsilon_c)\, BR(c \to \ell)\, A_c(\theta)\;) \times N_Z \times \epsilon(p,p_t) \\
& + N_{q\bar{q}}(p,p_t,\theta)\, f_{q\bar{q}\to \text{non prompt lepton}}(p,p_t,\theta)
\end{aligned}
$$

  where N_Z is the number of Z hadronic events used in the analysis, $\epsilon(p, p_t)$ is the detection efficiency of a (p, p_t) lepton, $f_{process}(p, p_t, \theta, \varepsilon)$ is the probability that a lepton from some *process* fills the (p, p_t, θ) box, $N_{q\bar{q}}(p, p_t, \theta)$being the number of background events in the bin; γ_q is the ratio $\Gamma(Z \to q\bar{q})/\Gamma(Z \to hadrons)$.

- The opposite side dileptons provides severe constraints on $(b \to l)\ ^2\gamma_b$ which is in fact $(b \to l)\ P_b$. As P_b is measured with the single lepton, this sample essentially contributes to disentangle the $BR(b \to l)$ value and then γ_b. This means for instance that a small number of opposite side dilepton events would give a small value of $BR(b \to l)$; then, the product of $BR(b \to l)\gamma_b$ being almost fixed by the single lepton sample, the value of γ_b would be large. But let us note the following: if we have some problem with the lepton tagging efficiency, this will essentially not reflect on the γ_b measurement. In fact the value of $BR(b \to l)$ will take the full effect of bad efficiency since the number of single leptons (dileptons) vary linearly (quadratically) with both efficiency and $BR(b \to l)$. So the almost 100% correlation between $BR(b \to l)$ and γ_b (see page 39) is really a correlation at the level of statistics (taken into account by the fit) while the correlation is small for systematical effects.

  This sample of opposite side dileptons splits into same charge and opposite charge dileptons. This additionnal source of information is used to extract the mixing value χ. The measurement of χ **is not** done in a separate fit and in the likelihood all the parameters (partial widths, branching ratios, fragmentation parameters, mixing and asymmetries) vary simultaneously. The number of same sign dileptons in a $(p_\otimes, p_{t\,min})$ box is given by:

$$\begin{aligned}
\mathrm{NDMS}\,(\mathrm{p}_\otimes, \mathrm{p_{t\,min}}) &= 2\chi(1-\chi)\,\mathrm{NBSO}\,(\mathrm{p}_\otimes, \mathrm{p_{t\,min}}) \\
&\quad + (1 - 2\chi(1-\chi))\,\mathrm{NBMS}\,(\mathrm{p}_\otimes, \mathrm{p_{t\,min}}) \\
&\quad + \mathrm{NFAKE_{same\ sign}}(\mathrm{p}_\otimes, \mathrm{p_{t\,min}})
\end{aligned}$$

where :

$$\begin{aligned}
\mathrm{NBSO}\,(\mathrm{p}_\otimes, \mathrm{p_{t\,min}}) &= N_Z \times \epsilon(p, p_t)\gamma_b \Big[BR(b \to \ell)^2\, f_{b\to\ell\ b\to\ell}(p_\otimes, p_{t\,min}, \varepsilon_b) \\
&\quad + BR(b \to \ell)\, BR(b \to \tau \to \ell) f_{b\to\ell\ b\to\tau\to\ell}(p_\otimes, p_{t\,min}, \varepsilon_b) \\
&\quad + BR(b \to \ell)\, BR(b \to W \to (\bar{c}s) \to \ell) \\
&\qquad f_{b\to\ell\ b\to W\to(\bar{c}s)\to\ell}(p_\otimes, p_{t\,min}, \varepsilon_b) \\
&\quad + BR(b \to \tau \to \ell)^2\, f_{b\to\tau\to\ell\ b\to\tau\to\ell}(p_\otimes, p_{t\,min}, \varepsilon_b) \\
&\quad + BR(b \to \tau \to \ell)\, BR(b \to W \to (\bar{c}s) \to \ell) \\
&\qquad f_{b\to\tau\to\ell\ b\to W\to(\bar{c}s)\to\ell}(p_\otimes, p_{t\,min}, \varepsilon_b) \\
&\quad + BR(b \to c \to \ell)^2\, f_{b\to c\to\ell\ b\to c\to\ell}(p_\otimes, p_{t\,min}, \varepsilon_b) \\
&\quad + BR(b \to W \to (\bar{c}s) \to \ell)^2 \\
&\qquad f_{b\to W\to(\bar{c}s)\to\ell\ b\to W\to(\bar{c}s)\to\ell}(p_\otimes, p_{t\,min}, \varepsilon_b) \Big]
\end{aligned}$$

$$\mathrm{NBMS}\,(\mathrm{p}_\otimes, \mathrm{p_{t\,min}}) = N_Z \times \epsilon(p, p_t)\gamma_b$$

$$
\begin{aligned}
&\Big[BR(b\to\ell)\,BR(b\to c\to\ell) f_{b\to\ell\ b\to c\to\ell}(p_\otimes, p_{t\,min}, \varepsilon_b)\\
&+\ BR(b\to\tau\to\ell)\,BR(b\to c\to\ell) f_{b\to\tau\to\ell\ b\to c\to\ell}(p_\otimes, p_{t\,min}, \varepsilon_b)\\
&+\ BR(b\to W\to(\bar{c}s)\to\ell)\,BR(b\to c\to\ell)\\
&\ f_{b\to W\to(\bar{c}s)\to\ell\ b\to c\to\ell}(p_\otimes, p_{t\,min}, \varepsilon_b)\Big]
\end{aligned}
$$

$$
\begin{aligned}
\mathrm{NFAKE}\,(\mathrm{p}_\otimes, \mathrm{p_{t\ min}}) \;=\;& N_Z \times \epsilon(p,p_t)\gamma_b \Big[BR(b\to\ell)\, f_{b\to\ell\ \mathrm{other}}(p_\otimes, p_{t\,min}, \varepsilon_b)\\
&+\ BR(b\to\tau\to\ell)\, f_{b\to\tau\to\ell\ \mathrm{other}}(p_\otimes, p_{t\,min}, \varepsilon_b)\\
&+\ BR(b\to c\to\ell)\, f_{b\to c\to\ell\ \mathrm{other}}(p_\otimes, p_{t\,min}, \varepsilon_b)\\
&+\ BR(b\to W\to(\bar{c}s)\to\ell)\, f_{b\to W\to(\bar{c}s)\to\ell\ \mathrm{other}}(p_\otimes, p_{t\,min}, \varepsilon_b)\Big]\\
&+\ N_Z \times \epsilon(p,p_t)\gamma_c \Big[BR(c\to\ell)\, f_{c\to\ell\ \mathrm{other}}(p_\otimes, p_{t\,min}, \varepsilon_c)\\
&+\ BR(c\to\ell)^2\, f_{c\to\ell\ c\to\ell}(p_\otimes, p_{t\,min}, \varepsilon_c)\Big]\\
&+\ N_{q\bar{q}}(p_\otimes, p_{t\,min})\, f_{q\bar{q}\to\text{non prompt lepton}}(p_\otimes, p_{t\,min})
\end{aligned}
$$

And the number of opposite sign dileptons in a $(p_\otimes, p_{t\,min})$ box is given by:

$$
\begin{aligned}
\mathrm{NDSO}\,(\mathrm{p}_\otimes, \mathrm{p_{t\ min}}) \;=\;& 2\chi(1-\chi)\,\mathrm{NBMS}\,(\mathrm{p}_\otimes, \mathrm{p_{t\ min}})\\
&+\ (1-2\chi(1-\chi))\,\mathrm{NBSO}\,(\mathrm{p}_\otimes, \mathrm{p_{t\ min}})\\
&+\ \mathrm{NFAKE}_{\text{opposite sign}}(\mathrm{p}_\otimes, \mathrm{p_{t\ min}})
\end{aligned}
$$

- The same side dileptons are used to measure $BR(b\to c\to l)$ (see previous section). This is due to the fact that the double semileptonic cascade from the b decay is proportionnal to $BR(b\to l)BR(b\to c\to l)\ \gamma_b = P_b \times BR(b\to c\to l)$.

  The same side dilepton sample is strongly dominated by the double cascade semileptonic b decays. Except the $J/\psi\to l^+l^-$ whose effect on our analysis is negligible, the main background to this analysis is produced by a prompt lepton from heavy quark decays associated to a misidentified lepton. Only the background associated to the $b\to l$ decay is important since we analyze the events in the $(p_\otimes,\ p_{tmin})$ plane.

  The other possible source of background is from photon materialisation and Dalitz pairs (or η decays) but this background is well controlled (see figure 5). Then the measurement of $BR(b\to c\to l)$ suffers from the systematical uncertainty on the background level. The number of dileptons in a $(p_\otimes, p_{t\,min})$ box is given by:

$$
\mathrm{NDSS}\,(\mathrm{p}_\otimes, \mathrm{p_{t\ min}}) \;=\; N_Z \times \epsilon(p,p_t)\gamma_b
$$

$$
\begin{aligned}
&\Big[BR(b\to\ell)\,BR(b\to c\to\ell) f_{b\to\ell\ b\to c\to\ell}(p_\otimes, p_{t\,min}, \varepsilon_b)\\
&+\ BR(b\to\tau\to\ell)\,BR(b\to c\to\ell) f_{b\to\tau\to\ell\ b\to c\to\ell}(p_\otimes, p_{t\,min}, \varepsilon_b)\\
&+\ BR(b\to W\to(\bar{c}s)\to\ell)\,BR(b\to c\to\ell)\\
&f_{b\to W\to(\bar{c}s)\to\ell\ b\to c\to\ell}(p_\otimes, p_{t\,min}, \varepsilon_b)\\
&+ BR(b\to\ell)\, f_{b\to\ell\ \text{other}}(p_\otimes, p_{t\,min}, \varepsilon_b)\\
&+\ BR(b\to\tau\to\ell)\, f_{b\to\tau\to\ell\ \text{other}}(p_\otimes, p_{t\,min}, \varepsilon_b)\\
&+\ BR(b\to c\to\ell)\, f_{b\to c\to\ell\ \text{other}}(p_\otimes, p_{t\,min}, \varepsilon_b)\\
&+\ BR(b\to W\to(\bar{c}s)\to\ell)\, f_{b\to W\to(\bar{c}s)\to\ell\ \text{other}}(p_\otimes, p_{t\,min}, \varepsilon_b)\Big]\\
&+\ N_Z\times\epsilon(p,p_t)\gamma_c BR(c\to\ell)\, f_{c\to\ell\ \text{other}}(p_\otimes, p_{t\,min}, \varepsilon_c)\\
&+\ N_{q\bar{q}}(p_\otimes, p_{t\,min})\, f_{q\bar{q}\to\text{non prompt lepton}}(p_\otimes, p_{t\,min})
\end{aligned}
$$

The total likelihood of the global fit can be written :

$$\mathcal{L} \;=\; \mathcal{L}^S + \mathcal{L}^{OS} + \mathcal{L}^{SS}$$

where :

- $\mathcal{L}^S$ = single lepton sample

$$\mathcal{L}^S \;=\; -\sum_{i}^{ee,\ \mu\mu,\ e\mu}\ \sum_{k=\cos\theta}^{\text{Forward,Backward}}\ \sum_{j} \text{Log}\left(\frac{x^S_{i,j,k}{}^{\,n^S_{i,j,k}}\, e^{-x^S_{i,j,k}}}{n^S_{i,j,k}!}\right)$$

$x^S_j = NS(p, p_t, \theta)$: predicted number of single leptons in bin j,
n^S_j is the observed one.

- $\mathcal{L}^{OS}$ = opposite side dilepton sample

$$\mathcal{L}^{OS} = -\sum_{i}^{ee,\ \mu\mu,\ e\mu\ \text{same sign, opposite sign}}\ \sum_{k}\ \sum_{j} \text{Log}\left(\frac{x^{OS}_{i,j,k}{}^{\,n^{OS}_{i,j,k}}\, e^{-x^{OS}_{i,j,k}}}{n^{OS}_{i,j,k}!}\right)$$

x^{OS}_j same sign = $NDMS(p_\otimes, p_{t\ \text{min}})$ Predicted number of opposite side same sign dileptons in bin j

x^{OS}_j opposite sign = $NDOS(p_\otimes, p_{t\ \text{min}})$ Predicted number of opposite side, opposite sign dileptons in bin j

n^{OS}_j same sign, opposite sign = the observed number

- $\mathcal{L}^{MS}$ = same side dilepton sample

$$\mathcal{L}^{MS} = -\sum_{i}^{ee,\ \mu\mu,\ e\mu}\ \sum_{j} \mathrm{Log}\ \frac{x_{i,j}^{MS}\ x_{i,j}^{MS}\ e^{-x_{i,j}^{MS}}}{x_{i,j}^{MS}!}$$

x_j^{MS} = $NDSS\,(p_{\otimes}, p_{t\ \mathrm{min}})$ predicted number of same side dilepton

n_j^{MS} = the observed number

6.5 Results of the global fit

The distributions of kinematical variables for the three samples of events are shown in figures 11, 12 and 13; they are presented with the results of the fit given in table 10 for 1990 and 1991 separately and the total statistics.

Parameter	e+μ '90 (Stat. error)	e+μ '91 (Stat. error)	e+μ '90+'91 (Stat. error)
$R(b)(\%)$	21.0±1.1	21.7±0.8	21.4±0.6
$R(c)(\%)$	18.3±1.0	17.3±0.7	17.7±0.6
$< x_b >$	0.704±0.006	0.701±0.005	0.702±0.003
$< x_c >$	$0.479^{+0.017}_{-0.006}$	$0.528^{+0.014}_{-0.012}$	$0.508^{+0.009}_{-0.015}$
$BR(b \to l)$	11.8±0.6	11.2±0.4	11.4±0.3
$BR(b \to c \to l)$	9.2±0.5	8.4±0.3	8.7±0.3
$\chi(\%)$	13.5±2.4	12.1±1.6	12.6±1.3
$A_c(\%)$	12.4±3.5	7.2±2.4	9.3±2.0
$A_b^{obs.}(\%)$	8.7±1.6	5.4±1.1	6.8±0.9
$A_b^{cor.}(\%)$	12.0±2.3	7.1± 1.5	9.1±1.3

Table 10: Results of the global analysis of single and dilepton events

$$A_b^{cor} = \frac{A_b^{obs}}{1-2\chi}$$

The source of systematical errors are given in table 11. They are quite conservative.

Source	variation
e-efficiency	$\pm 3\%$
μ-efficiency	$\pm 3\%$
γ conv.	$\pm$ 2 %
e-misid.	$\pm$ 10%
μ-decay	$\pm 3\%$
μ punch-through	$\pm$ 20%
$BR(c \rightarrow l)$	± 0.5
$BR(B \rightarrow \tau)$	$\pm$ 0.8
$b \rightarrow W \rightarrow c$	$\pm 50\%$
$b \rightarrow J/\psi$	$\pm$ 15%
$BR(b \rightarrow u)$	(1.5-4.5)%
Bkgr. charg asymetry	$\pm$ 4 %
$A_{FB}^{background}$	$\pm$ 1 σ

Table 11: Sources of systematical error in the global analysis

Par.	e-eff.	μ-eff	γ	e-mis.	μ-dec.	μ-p.t.	$A_{charge}^{back.}$
$R(b)$	0.02	0.02	0.02	0.02	0.06	0.28	
$R(c)$	0.47	0.40	0.18	0.24	0.18	1.03	
$BR(b \rightarrow l)$	0.18	0.15	0.01	0.08	0.04	0.16	
$BR(b \rightarrow c \rightarrow l)$	0.15	0.18	0.02	0.01	0.05	0.28	
$< x_b >$	0.001	0.001	0.000	0.000	0.000	0.001	
$< x_c >$	0.023	0.009	0.009	0.003	0.005	0.005	
χ	0.02	0.07	0.02	0.005	0.05	0.3	0.05
$A_b^{obs.} \equiv A_b^{cor.}$	0.05	0.02	0.007	0.001	0.008	0.003	
A_c	0.16	0.07	0.10	0.114	0.124	0.42	

Table 12: Systematics (1^{st} part)

In addition to the systematics quoted in this table 11 we have used an other fragmentation model than the traditional one of Peterson [18] (the correspon-

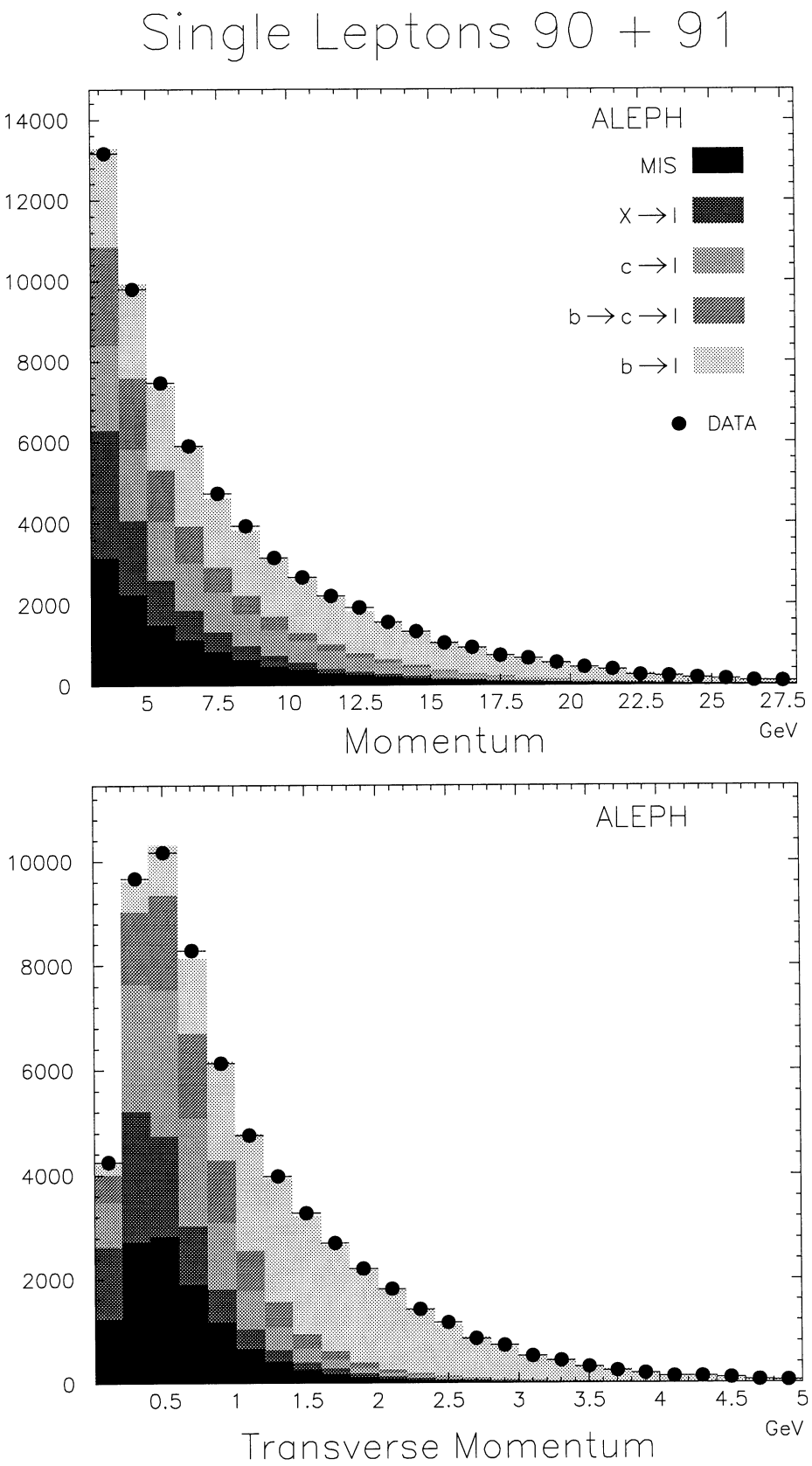

Figure 11: P and P_t distributions

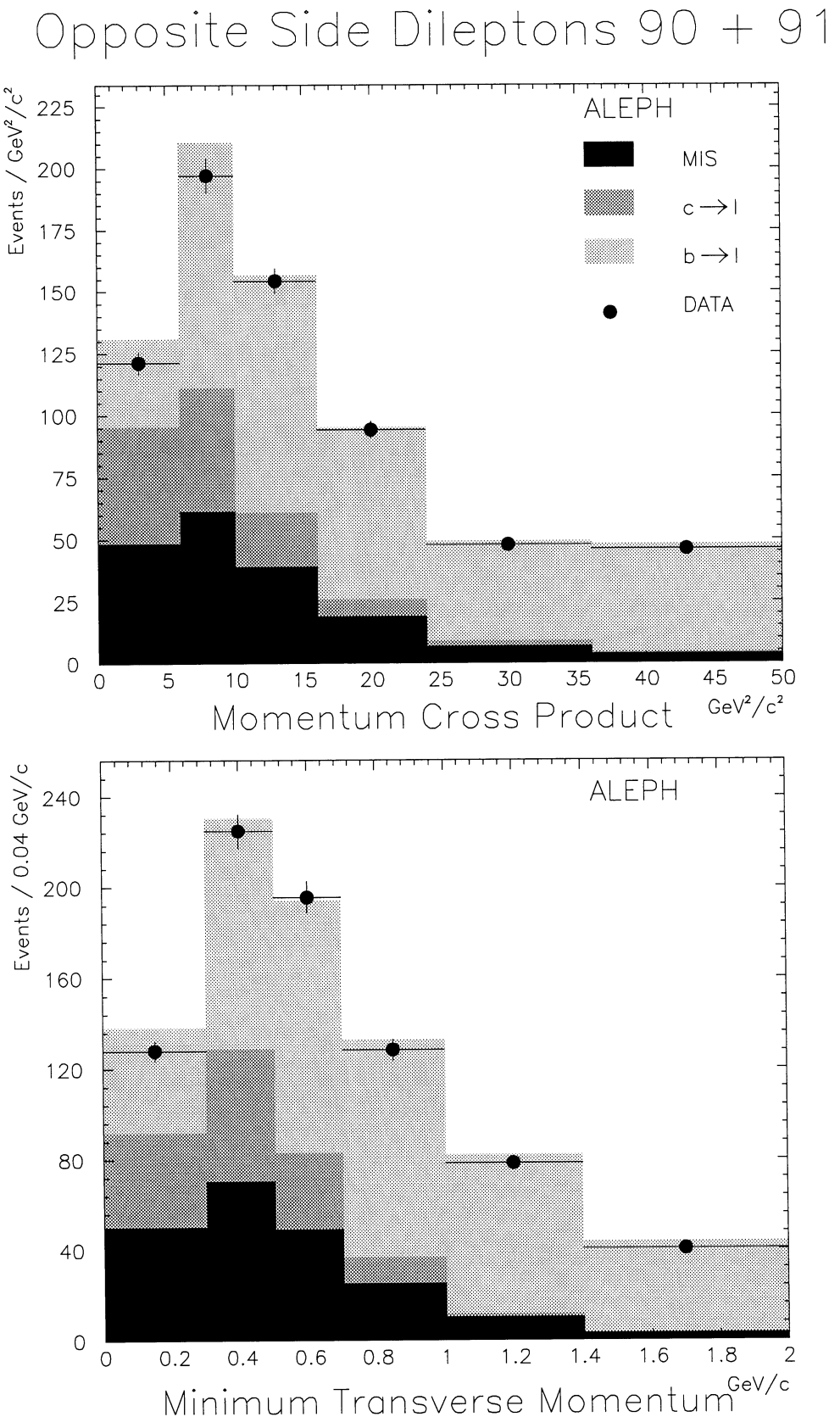

Figure 12: P_{cross} *and* P_{tmin} **distributions for Opposite Side dileptons**

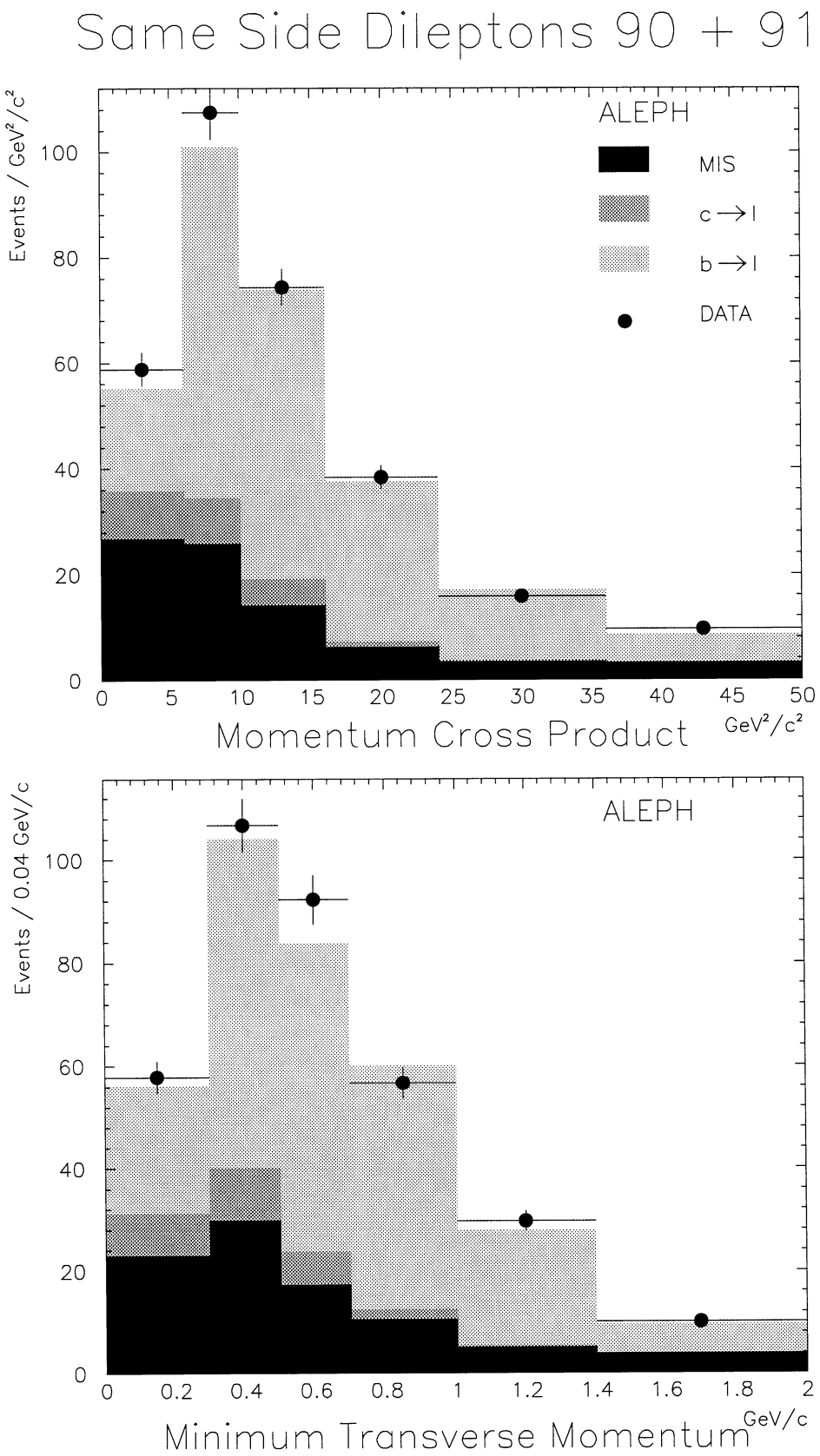

Figure 13: P_{cross} *and* P_{tmin} **distributions for Same Side dileptons**

Par.	$c \to l$	$B \to \tau$	$b \to W \to c$	$b \to J/\psi$	$b \to u$	$A_{FB}^{back.}$	Total
$R(b)$	0.098	0.03	0.06	0.03	0.22		0.38
$R(c)$	0.93	0.06	0.5	0.06	0.06		1.61
$BR(b \to l)$	0.048	0.03	0.03	0.02	0.038		0.31
$BR(b \to c \to l)$	0.015	0.09	0.2	0.06	0.41		0.6
$< x_b >$	0.000	0.001	0.001	0.002	0.004		0.005
$< x_c >$	0.001	0.006	0.027	0.001	0.027		0.056
χ	0.014	0.19	0.48	0.04	0.25		0.66
$A_b^{obs.}$	0.002	0.007	0.04	0.023	0.024	0.07	0.10
$A_b^{cor.}$	0.002	0.045	0.10	0.023	0.004	0.07	0.14
A_c	0.035	0.107	0.475	0.019	0.15	1.38	1.55

Table 13: Systematics (2^{nd} part)

dance, in our MC, between the parameters of this model - ϵ_b, ϵ_c - and $< X_E >$ is given figures 14 and 15) :

$$D_Q^H(z) = \frac{N}{z(1-\frac{1}{z}-\frac{\epsilon_Q}{1-z})^2}$$

the model of Kartvelishvili et al. [20] ((table 14) (the correspondance, in our MC, between the parameters of this model - α_b, α_c - and $< X_E >$ is given figures 16 and 17)

$$D_Q^H(z) = N z^{\alpha_q}(1-z)$$

Parameter	Peterson	Kartvelishvili
$R(b)$	21.7	21.7
$R(c)$	17.3	16.7
$< x_b >$	0.701	0.700
$< x_c >$	0.528	0.539
$BR(b \to l)$	11.2	11.1
$BR(b \to c \to l)$	8.4	8.4
χ	12.1	12.1
A_c	7.2	7.1
$A_b^{corr.}$	7.1	7.1

Table 14: Influence of the fragmentation modelisation ('91 data)

Essentially b physics is not affected (table 14).

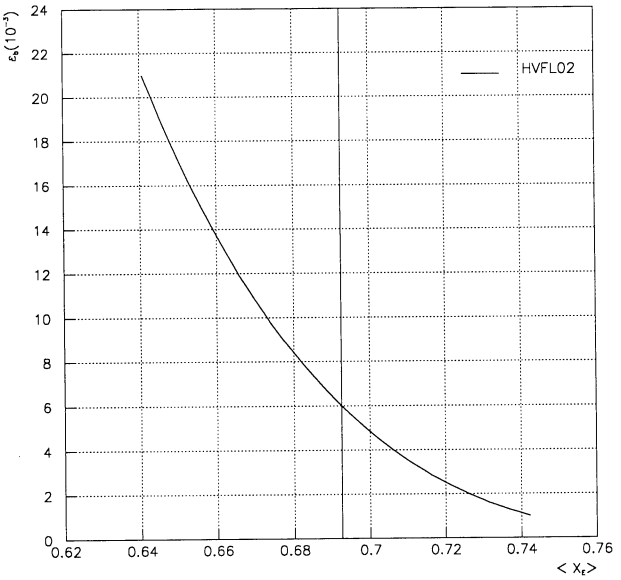

Figure 14: Evolution of $< X_E >$ as a function of ϵ_b for the beauty in the Peterson model

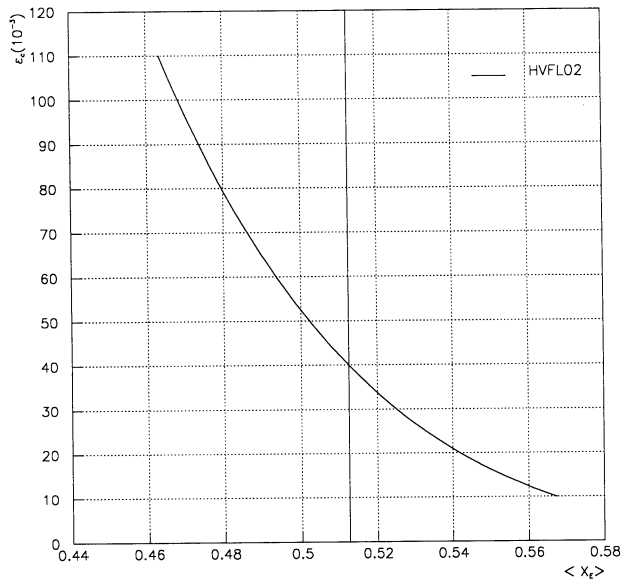

Figure 15: Evolution of $< X_E >$ as a function of ϵ_c for the charm in the Peterson model

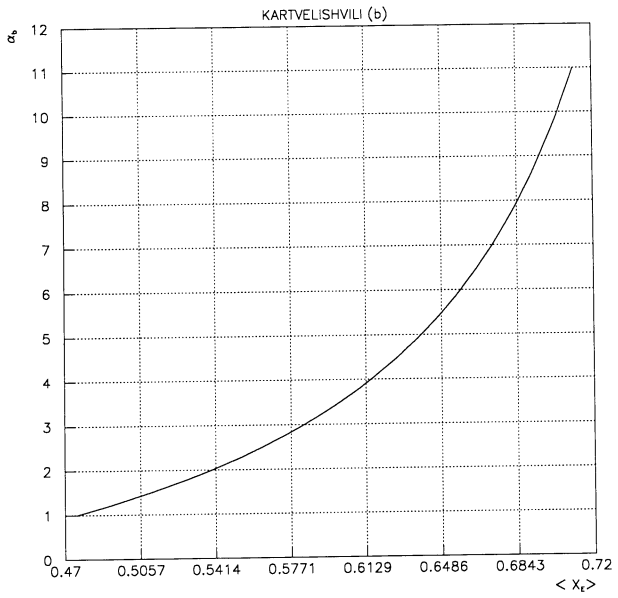

Figure 16: Evolution of $< X_E >$ as a function of α_b for the beauty in the Kartvelishvili model

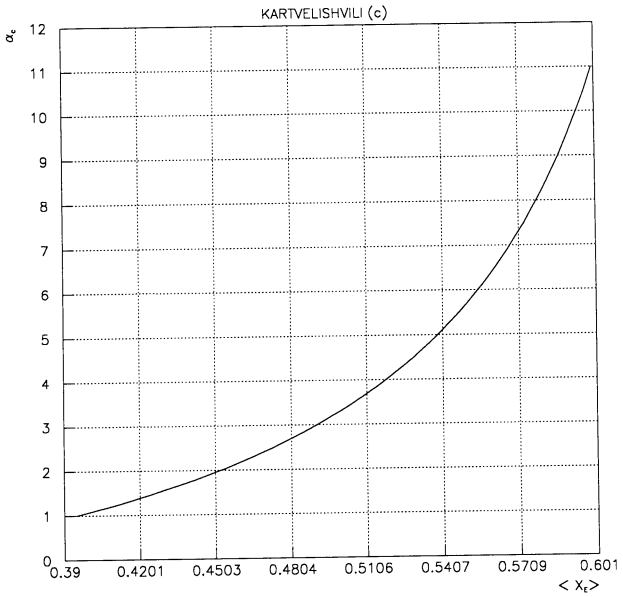

Figure 17: Evolution of $< X_E >$ as a function of α_c for the charm in the Kartvelishvili model

We have also studied the error induced by the modelisation of the lepton spectrum in the B rest frame. What we have done is to weight the generated events by the best parametrisation found by CLEO and ARGUS [11] by using the ISGW model [10]. In this model the influence of higher mass charmed states in B decays (D^{**} , $D^*\pi$ effects) is introduced. The best fit of ARGUS and CLEO corresponds to a total fraction of 21 % D, 47% D^*, 32% D^{**}. The results are given table 15.

Parameter	e+μ '90 (Stat. error)	e+μ '91 (Stat. error)	e+μ '90+'91 (Stat. error)
$R(b)(\%)$	21.4±1.1	22.2±0.8	21.9±0.6
$R(c)(\%)$	18.0±1.0	16.6±0.6	17.2±0.5
$< x_b >$	0.725±0.006	0.722±0.005	0.723±0.003
$< x_c >$	$0.477^{+0.017}_{-0.006}$	$0.533^{+0.014}_{-0.012}$	$0.508^{+0.009}_{-0.015}$
$BR(b \to l)$	12.3±0.6	11.6±0.4	11.9±0.3
$BR(b \to c \to l)$	7.9±0.4	7.2±0.3	7.5±0.3
$\chi(\%)$	15.1±2.4	13.7±1.6	14.3±1.4
$A_c(\%)$	14.1±3.7	8.4±2.5	10.7±2.1
$A_b^{obs.}(\%)$	8.7±1.6	5.4±1.1	6.8±0.9
$A_b^{cor.}(\%)$	12.5±2.4	7.5± 1.5	9.5±1.3

Table 15: Results of the "global" fit with the ISGW model

Here also the quoted error is quite conservative. The effect on γ_b is ± 1 % systematics if we choose the average between these 2 models.

The main affected parameters are : $< X_b >$ and $(b \to c \to l)$ and correlatively χ is affected; this reflects on A_b^{corr}. This is mainly due to the fact the $BR(b \to l)$ and $BR(b \to c \to l)$ have changed and when χ is computed with these new branching ratio, we obtain a new value for χ. The aim to measure χ in this analysis is to correctly measure A_b; then we have to optimise our χ measurement to achieve this goal. To decrease this model dependence we restrict the measurement of χ in a region where the $(b \to c \to l)$ contribution is not so important. The best optimum is find for a p_t cut greater than 1 GeV. The new systematical errors concerning χ and $A_b^{cor.}$ are quoted in table 16. The fact to restrict the analysis to a quite large p_t is very specific to mixing measurement. In fact, when restricting the p_t region we put in competition two processes: $b \to l\bar{b} \to l$ and $b \to l\bar{b} \to \bar{c} \to l$ so that the weight of $b \to c \to l$ is small. Going to low p_t the relative importance of $b \to c \to l$ increases rapidly due to $b \to c \to l\bar{b} \to \bar{c} \to l$.

The final results are given in table 17 and 18 for the 2 models. Finally we show in table 21 what are the correlations between all the parameters measured in this

Par.	e-eff.	μ-eff	γ	e-mis.	μ-dec.	μ-p.t.	$A_{charge}^{back.}$
χ	0.002	0.04	0.01	0.005	0.03	0.21	0.05
$A_b^{cor.}$	0.05	0.02	0.007	0.001	0.008	0.003	0.
Par.	$c \to l$	$B \to \tau$	$b \to W \to c$	$b \to J/\psi$	$b \to u$	$A_{FB}^{back.}$	Total
χ	0.004	0.07	0.20	0.04	0.16	0.	0.35
$A_b^{cor.}$	0.001	0.026	0.091	0.023	0.004	0.07	0.13

Table 16: New systematics on χ and A_b for the determination of χ with $p_t \geq 1.$ GeV

global analysis. There is nothing surprising in this table and the correlations are automatically propagated in the statistical errors.

Parameter	e+μ '90 (Stat. error)	e+μ '91 (Stat. error)	e+μ '90+'91 (Stat. error)
$R(b)(\%)$	21.2±1.1	21.7±0.8	21.5±0.6
$R(c)(\%)$	18.1±1.0	17.3±0.7	17.6±0.6
$< x_b >$	0.704±0.006	0.701±0.005	0.702±0.003
$< x_c >$	$0.479^{+0.017}_{-0.006}$	$0.528^{+0.014}_{-0.012}$	$0.508^{+0.009}_{-0.015}$
$BR(b \to l)$	11.7±0.6	11.2±0.4	11.4±0.3
$BR(b \to c \to l)$	9.3±0.5	8.4±0.3	8.7±0.3
$\chi(\%)$	8.9±2.3	12.7±1.7	11.1±1.4
$A_c(\%)$	12.5±3.5	7.2±2.4	9.3±2.0
$A_b^{obs.}(\%)$	8.7±1.6	5.4±1.1	6.8±0.9
$A_b^{cor.}(\%)$	10.7±2.0	7.2± 1.6	8.7±1.2

Table 17: Results of the "global" fit

Parameter	e+μ '90 (Stat. error)	e+μ '91 (Stat. error)	e+μ '90+'91 (Stat. error)
$R(b)(\%)$	21.6±1.1	22.2±0.8	22.0±0.6
$R(c)(\%)$	17.8±1.0	16.6±0.7	17.1±0.5
$< x_b >$	0.725±0.006	0.722±0.005	0.723±0.003
$< x_c >$	$0.477^{+0.017}_{-0.006}$	$0.533^{+0.014}_{-0.012}$	$0.508^{+0.009}_{-0.015}$
$BR(b \to l)$	12.1±0.6	11.6±0.4	11.8±0.3
$BR(b \to c \to l)$	8.0±0.4	7.2±0.3	7.5±0.2
$\chi(\%)$	9.9±2.3	13.5±1.7	12.0±1.4
$A_c(\%)$	14.2±3.7	8.4±2.5	10.7±2.1
$A_b^{obs.}(\%)$	8.7±1.6	5.4±1.1	6.8±0.9
$A_b^{cor.}(\%)$	10.9±2.0	7.5± 1.6	9.0±1.2

Table 18: Results of the "global" fit with the ISGW model

We have measured the forward-backward asymmetry of $Z^0 \to b\bar{b}$ and $Z^0 \to c\bar{c}$ events at seven energy points in the global fit (table 20 and 22). To do that the other parameters are fitted simultaneously with all the energy points and only A_{FB}^b and A_{FB}^c are extracted at each point. The results are listed in table 20 for the two models. The hard spectrum refers to the Altarelli model and the soft one to the ISGW one. The A_{FB}^b measured is direcly corrected by the measured value of the mixing parameter inside the fit, and the main systematics due to the mixing is directly included, as the other one, in the statistical error.

We have also measured the forward-backward asymmetry of $Z^0 \to b\bar{b}$ events at seven energy points in the global fit by using a relation between A_{FB}^b and A_{FB}^c as A_{FB}^c suffers for a lake of statistics. The values of the ratio κ between A_{FB}^b and A_{FB}^c used at the various energy points are taken from Expostar [21], and are listed in table 23. The values of the A_{FB}^b are given in table 24.

		Statistical Error	Systematic Error
	$\Gamma(b\bar{b})/\Gamma(had)$		
hard spectrum	0.215	0.0062	0.0038
soft spectrum	0.220	0.0063	0.0038
	$\Gamma(c\bar{c})/\Gamma(had)$		
hard spectrum	0.176	0.0055	0.0161
soft spectrum	0.171	0.0054	0.0161
	$< X_b >$		
hard spectrum	0.702	0.004	0.005
soft spectrum	0.723	0.004	0.005
	$< X_c >$		
hard spectrum	0.508	0.083	0.06
soft spectrum	0.508	0.083	0.06
	$\mathrm{Br}(b \to l\nu\mathrm{X})$		
hard spectrum	0.114	0.0033	0.0031
soft spectrum	0.118	0.0033	0.0031
	$\mathrm{Br}\ (b \to c \to l)$		
hard spectrum	0.087	0.0025	0.0060
soft spectrum	0.075	0.0023	0.0060
	χ		
hard spectrum	0.111	0.014	0.005
soft spectrum	0.120	0.014	0.005
	$\mathrm{A}^{b}_{\mathrm{FB}}$		
hard spectrum	0.087	0.0124	0.0014
soft spectrum	0.090	0.0125	0.0014
	$\mathrm{A}^{c}_{\mathrm{FB}}$		
hard spectrum	0.093	0.0200	0.0155
soft spectrum	0.107	0.0208	0.0155

Table 19: Global analysis results, Includes all beam energies.

	A_{FB}^b	Statistical Error	Systematic Error
PEAK - 2.8:			
hard spectrum	0.076	0.100	0.001
soft spectrum	0.078	0.103	0.001
PEAK - 1.8:			
hard spectrum	0.027	0.072	0.001
soft spectrum	0.036	0.074	0.001
PEAK - 1.0:			
hard spectrum	0.062	0.054	0.001
soft spectrum	0.064	0.055	0.001
PEAK:			
hard spectrum	0.086	0.014	0.001
soft spectrum	0.088	0.014	0.001
PEAK + 0.8:			
hard spectrum	0.065	0.045	0.001
soft spectrum	0.066	0.046	0.001
PEAK + 1.8:			
hard spectrum	0.123	0.058	0.001
soft spectrum	0.126	0.059	0.001
PEAK + 2.5:			
hard spectrum	0.096	0.071	0.001
soft spectrum	0.098	0.073	0.001

Table 20: Global fit analysis results for A_{FB}^b , after mixing correction

ρ	Γ_c	$< X_b >$	$< X_c >$	$(b \to l)$	$(b \to c \to l)$	χ	A_{FB}^b	A_{FB}^c
Γ_b	-0.478	0.229	-0.048	-0.942	-0.378	-0.070	-0.004	0.050
Γ_c		0.057	0.494	0.471	-0.311	0.087	-0.009	-0.070
$< X_b >$			0.120	-0.352	-0.270	-0.007	-0.003	0.000
$< X_c >$				0.149	-0.295	0.048	-0.039	-0.002
$(b \to l)$					0.246	0.090	0.001	-0.036
$(b \to c \to l)$						-0.074	0.002	-0.013
χ							0.214	-0.003
A_{FB}^b								0.213

Table 21: Global analysis covariance matrix

	A^c_{FB}	Statistical Error	Systematic Error
PEAK - 2.8:	0.028	0.165	0.016
PEAK - 1.8:	0.259	0.119	0.016
PEAK - 1.0:	0.050	0.088	0.016
PEAK:	0.104	0.022	0.016
PEAK + 0.8:	0.049	0.073	0.016
PEAK + 1.8:	0.032	0.096	0.016
PEAK + 2.5:	0.070	0.114	0.016

Table 22: Global fit analysis results for A^c_{FB}

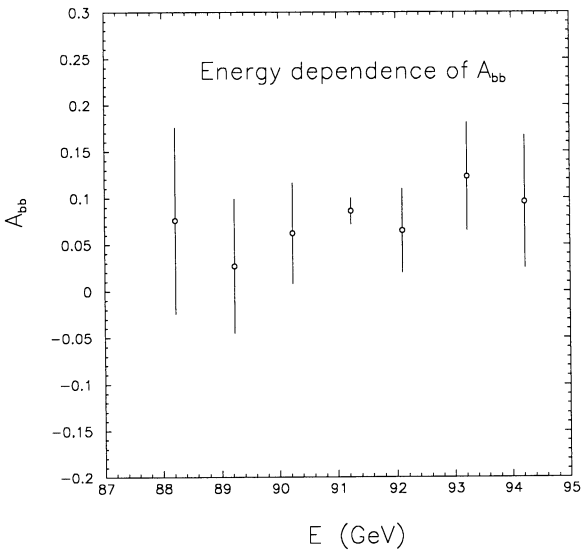

Figure 18: Extracted A^b_{FB} as a function of energy. The plotted errors are statistical only.

Energy Point	κ
PEAK - 2.8:	-0.18
PEAK - 1.8:	-0.67
PEAK - 1.0:	10.0
PEAK:	1.3
PEAK + 0.8:	1.1
PEAK + 1.8:	0.91
PEAK + 2.5:	0.83

Table 23: Values of the ratio κ at the various energy points, from Expostar

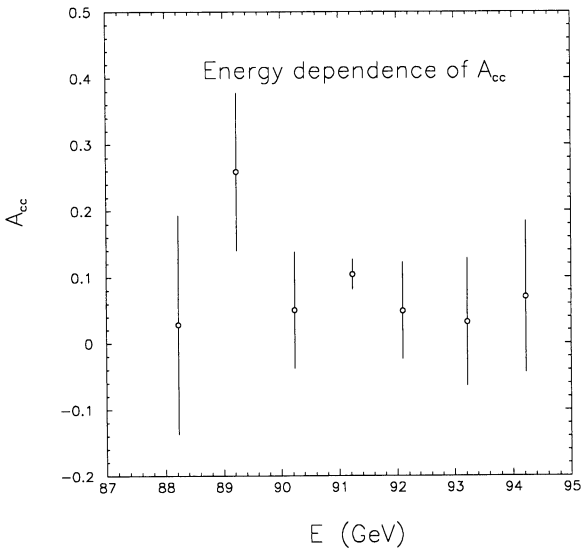

Figure 19: Extracted A_{FB}^{c} as a function of energy. The plotted errors are statistical only.

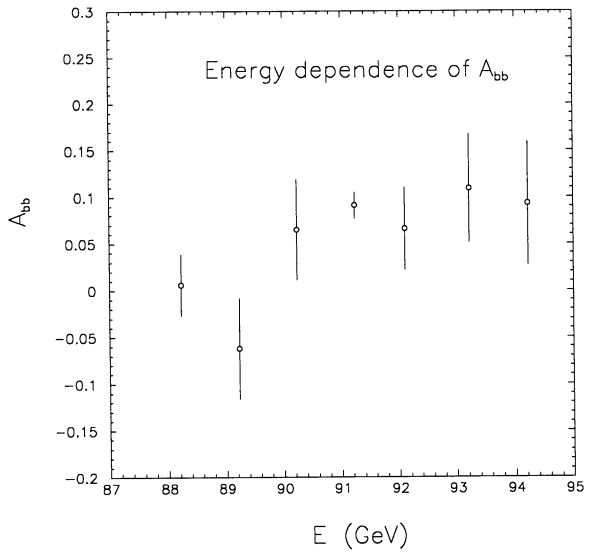

Figure 20: Extracted A_{FB}^{b} as a function of energy. The A_{FB}^{c} is fixed according to the SM relation. The plotted errors are statistical only.

	A_{FB}^b	Statistical Error	Systematic Error
PEAK - 2.8:	0.006	0.033	0.010
PEAK - 1.8:	- 0.062	0.054	0.010
PEAK - 1.0:	0.065	0.054	0.010
PEAK:	0.091	0.014	0.010
PEAK + 0.8:	0.066	0.044	0.010
PEAK + 1.8:	0.109	0.058	0.010
PEAK + 2.5:	0.093	0.066	0.010

Table 24: Global fit analysis results for A_{FB}^b when A_{FB}^c is related to A_{FB}^b by the SM

As a final check we have looked for possible variations of the results with p_t. Let us recall that no p_t dependance has been observed in the inclusive single lepton analysis (see previous section). Here also the analysis is done with '91 data due to the limited MC statistics available to analyze '90 data which could cause problem at high p_t. The results are summarized in table 25. It indicates an increase of R_b corresponding to a decrease of $BR(b \to l)$, the product of these two parameters being quite stable. Considering the two regions $p_t > 1.25$ GeV/c and $p_t < 1.25$ GeV/c as two independant sources of informations we compute that this p_t variation is at the level of a 2 σ statistical effect. Then at the moment being, we have no significant evidence of a systematical problem.

$P_t >$	0.	0.25	0.5	0.75
$R(b)$	21.7±0.5	21.5±0.5	22.0±0.6	22.4±0.7
$BR(b \to l)$	11.2±0.3	11.3±0.3	11.1±0.3	10.9±0.4
$< X_b >$	0.701±0.005	0.701±0.005	0.701±0.005	0.699±0.005
$R(b)$ $(b \to l)$	243.4	243.5	243.4	242.9
$P_t >$	1.0	1.25	1.5	
$R(b)$	23.5 ± 0.9	23.8 ± 1.2	23.4 ± 1.5	
$BR(b \to l)$	10.2±0.5	10.3±0.6	10.6±0.7	
$< X_b >$	0.703±0.005	0.697±0.006	0.691±0.007	
$R(b)$ $(b \to l)$	241.1	243.9	247.5	

Table 25: Variation of Γ_b and $BR(b \to l)$ with respect to p_t in the global fit '91 data e + μ with the Altarelli model.

7 Conclusion

We have presented a global analysis of single and dilepton events to extract properties of the coupling of Z to $b\bar{b}$ and $c\bar{c}$ final states (table 26). Essentially b physics in on a good shape for both R_b and A_b: A_b provides a measurement of $sin^2\theta_W$ at the level of 3 per 1000 and R_b is compatible with the standard model. The branching ratio $BR(b \rightarrow l)$ is larger than the value measured in the first generation of LEP measurements and becomes more consistent with the theoretical expectations (let us mention that the recent analysis from CLEO and ARGUS tend also to increase the value of $BR(b \rightarrow l)$ due to the large effect of higher mass charmed final states). We give a first measurement of $BR(b \rightarrow c \rightarrow l)$ but the interest of this measurement is decreased by the large effect of modelisation. The fragmentation of b is confirmed to be hard; here also the problem is related to modelisation of the semileptonic b hadron decays.

Generally, charm measurements remain limited by statistics but R_c is strongly limited by our knowledge of background. It is clear that for future we will have to work for a better understanding of backgrounds to follow in a decent way the increase of statistics.

Parameter	e+μ '90+'91	Statistical Uncertainty	Systematic Uncertainty	Modelisation Uncertainty
$R(b)(\%)$	21.7	0.62	0.38	0.23
$R(c)(\%)$	17.4	0.55	1.61	0.27
$< x_b >$	0.712	0.004	0.005	0.010
$< x_c >$	0.508	0.083	0.060	0.000
$BR(b \rightarrow l)$ (%)	11.6	0.33	0.31	0.20
$BR(b \rightarrow c \rightarrow l)(\%)$	8.1	0.25	0.60	0.61
$\chi(\%)$	11.5	1.40	0.50	0.44
$A_c(\%)$	10.0	2.04	1.55	0.72
$A_b^{cor.}(\%)$	8.8	1.24	0.14	0.12

Table 26: Final results of the "global" fit

References

[1] D. Abbaneo *et al.*, Aleph Note in preparation.

[2] D. Abbaneo *et al.*, Aleph Note 92-101

[3] P. Marotte - PhD Thesis - LAL Orsay.

[4] M. Bardadin *et al.* - Aleph Note 87-43.
Y. Saadi - PhD Thesis - Université de Clermont.

[5] T. Sjostrand and M. Bengtsson, The LUND Monte Carlo Programs, CERN long write-up, 1 November 1989.

[6] J.E. Campagne and R. Zitoun, Z. Phys. C **43** (1989) 469.

[7] M. Bauer, B. Stech, M. Wirbel - Z. Phys. C **34** (1987) 103.

[8] H. Schroder - DESY 88-101.
H. Albrecht *et al.* - Z. Phys. C **42** (1989) 519.

[9] M. Voloshin and V. Zakharov - Phys. Rev. Lett. 45 (1980) 688.

[10] J.G. Korner and G.A. Schuler - Z. Phys. C **38** (1988) 511.
W. Wirbel, B. Stech, M. Bauer - Z. Phys. C **29** (1985) 637.
N. Isgur, D. Scora, B. Grinstein, M.B. Wise - Phys. ReV. **D39** (1989) 799.

[11] ARGUS Coll. - H. Albrecht *et al.* - DESY 90-088.
CLEO Coll. - S. Henderson *et al.*, CLNS 91/1101, CLEO 91-7.

[12] B. Gittelman and S. Stone - CLNS 87/81.

[13] C.A. Dominguez and N. Paver - Z. Phys. C **41** (1988) 217.
B. Grinstein, N. Isgur, M.B. Wise - CALT-68-1311.
M. Bauer and M. Wirbel - Z. Phys. C **42** (1989) 671.

[14] E. Barberio *et al.* - PHOTOS a universal Monte Carlo for QED radiative corrections in decays - CERN-TH-5857/90.

[15] D. Atwood and W.J. Marciano - Radiative corrections and semileptonic B decays - Phys. Rev. **D41** (1990) 1736.

[16] M. Cattaneo and D. Colling - ALEPH 92-141. This note also contains a comparison of the two approaches.

[17] G. Altarelli *et al.* - N. Phys. **B208** (1982) 365.

[18] C. Peterson *et al.* - Phys. Rev **D27** (1983) 105.

[19] A.J. Weir *et al.*- MARK II Coll. - Phys. Lett. **B240** (1990) 289.

[20] V. G. Kartvelishvili, A. K. Likhoded and V. A. Petrov - Phys. Lett. **B78** (1978) 615.

[21] D. Levinthal *et al.* (ALEPH note) ALEPH 91-3.